

Preparation and Degradation of Rhodium and Iridium Diolefin Catalysts for the Acceptorless and Base-Free Dehydrogenation of Secondary Alcohols

María L. Buil, Alba Collado, Miguel A. Esteruelas,* Mar Gómez-Gallego, Susana Izquierdo, Antonio I. Nicasio, Enrique Oñate, and Miguel A. Sierra*

Cite This: *Organometallics* 2021, 40, 989–1003

Read Online

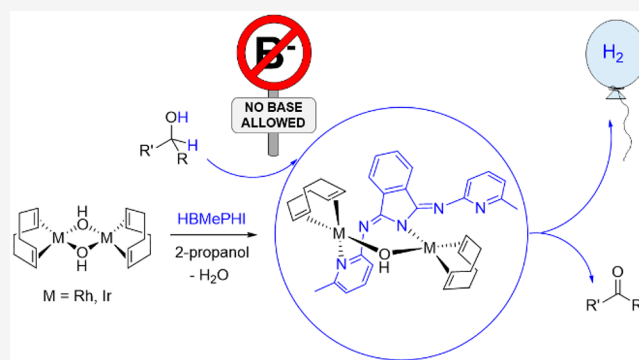
ACCESS |

Metrics & More

Article Recommendations

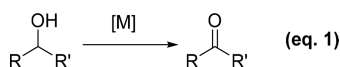
Supporting Information

ABSTRACT: Rhodium and iridium diolefin catalysts for the acceptorless and base-free dehydrogenation of secondary alcohols have been prepared, and their degradation has been investigated, during the study of the reactivity of the dimers $[M(\mu\text{-Cl})(\eta^4\text{-C}_8\text{H}_{12})_2]$ ($M = \text{Rh}$ (1), Ir (2)) and $[M(\mu\text{-OH})(\eta^4\text{-C}_8\text{H}_{12})_2]$ ($M = \text{Rh}$ (3), Ir (4)) with 1,3-bis(6'-methyl-2'-pyridylimino)isoidoline (HBMePHI). Complex 1 reacts with HBMePHI, in dichloromethane, to afford equilibrium mixtures of 1, the mononuclear derivative $\text{RhCl}(\eta^4\text{-C}_8\text{H}_{12})\{\kappa^1\text{-N}_{\text{py}}\text{-(HBMePHI)}\}$ (5), and the binuclear species $[\text{RhCl}(\eta^4\text{-C}_8\text{H}_{12})_2]\{\mu\text{-N}_{\text{py}}\text{N}_{\text{py}}\text{-(HBMePHI)}\}$ (6). Under the same conditions, complex 2 affords the iridium counterparts $\text{IrCl}(\eta^4\text{-C}_8\text{H}_{12})\{\kappa^1\text{-N}_{\text{py}}\text{-(HBMePHI)}\}$ (7) and $[\text{IrCl}(\eta^4\text{-C}_8\text{H}_{12})_2]\{\mu\text{-N}_{\text{py}}\text{N}_{\text{py}}\text{-(HBMePHI)}\}$ (8). In contrast to chloride, one of the hydroxide groups of 3 and 4 promotes the deprotonation of HBMePHI to give $[M(\eta^4\text{-C}_8\text{H}_{12})_2](\mu\text{-OH})\{\mu\text{-N}_{\text{py}}\text{N}_{\text{iso}}\text{-(BMePHI)}\}$ ($M = \text{Rh}$ (9), Ir (10)), which are efficient precatalysts for the acceptorless and base-free dehydrogenation of secondary alcohols. In the presence of KO^tBu , the $[\text{BMePHI}]^-$ ligand undergoes three different degradations: alcoholysis of an exocyclic isoidoline-N double bond, alcoholysis of a pyridyl-N bond, and opening of the five-membered ring of the isoidoline core.



INTRODUCTION

Ketones are a pivotal class of compounds, which can be easily transformed to diverse building blocks including (among others) imines, oximes, amines, and alkenes, the oxidation of alcohols being one of the most representative methods for their preparation.¹ Traditionally, stoichiometric amounts of chromium- and manganese-based reagents have been used for this purpose.^{1a} As a consequence of the large amounts of noxious waste generated, these methods have been gradually replaced by transition-metal catalysis operating under more environmentally friendly oxidants such as O_2 and H_2O_2 .² In the last few years, a further step was taken with the transition-metal-catalyzed acceptorless alcohol dehydrogenation, which does not need the use of oxidants (eq 1). The procedure



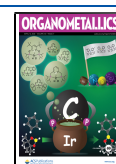
displays three environmental advantages: it offers an oxidation procedure for the synthesis of carbonyl compounds, minimizing waste formation, it is a promising approach to the production of hydrogen from biomass, and it provides a direct connection with the research on hydrogen storage and transport in organic liquids.³ The dehydrogenation of alcohols

is generally endothermic at room temperature but can be performed under mild conditions, for instance refluxing toluene in open systems, since the hydrogen elimination acts as a driving force of the reaction.⁴

Strongly basic media have generally been necessary for the operation of many catalysts, in particular with cationic compounds or precursors bearing halide ligands. The base cocatalyzes the dehydrogenation to generate an alkoxide, which binds to the metal and evolves into the carbonyl compound by β -hydrogen elimination.⁵ To prevent the waste generated by the base, the development of precursors operating under base-free conditions is receiving great attention.⁶ They coordinate ligands, being engaged in the deprotonation step. The basic center usually resides in the first metal coordination sphere⁷ and sometimes in a remote position.⁸

Received: February 4, 2021

Published: March 31, 2021



Scheme 1. Sequential N–H and C–H Activations of the Isoindoline Core of HBMePHI

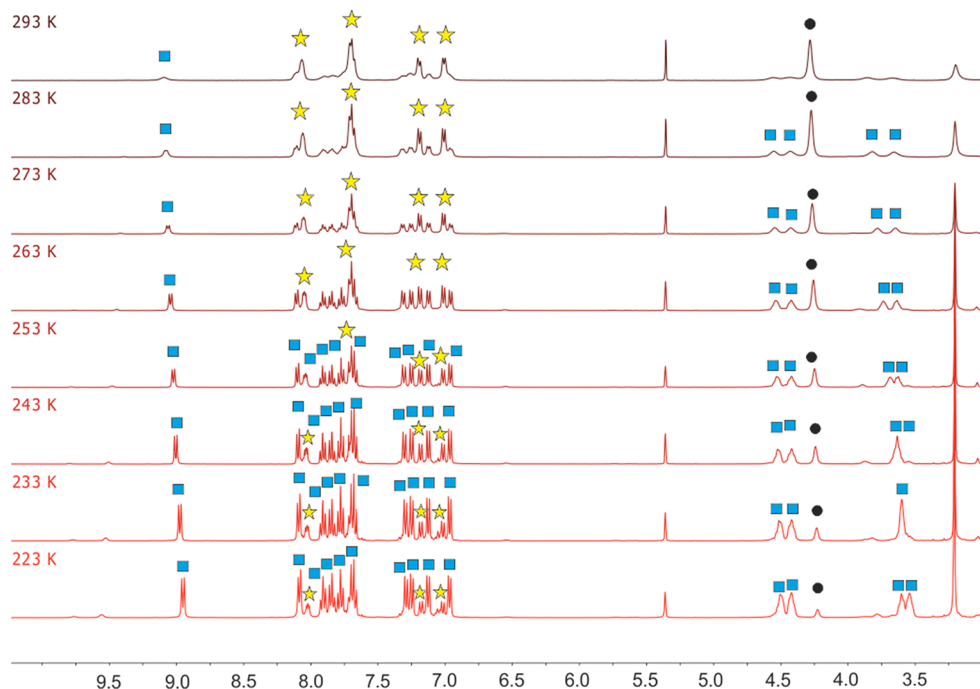
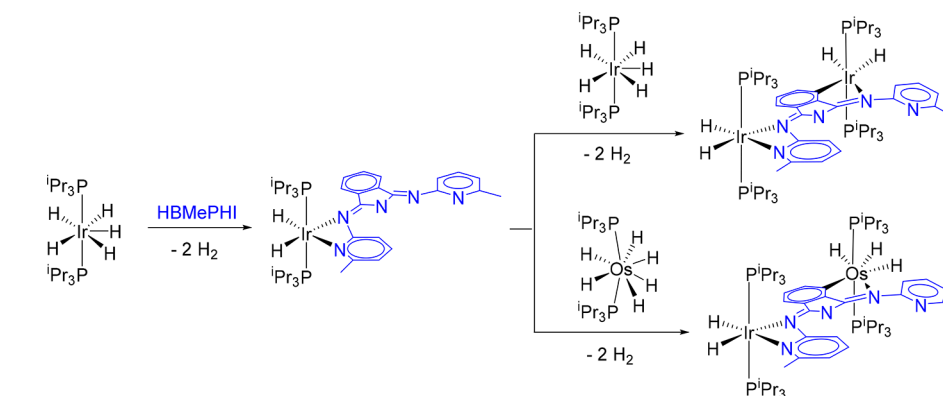


Figure 1. ^1H NMR spectra as a function of the temperature of the equilibrium shown in Scheme 2: blue ■, 5; yellow ☆, L; and black ●, 1 (in CD_2Cl_2).

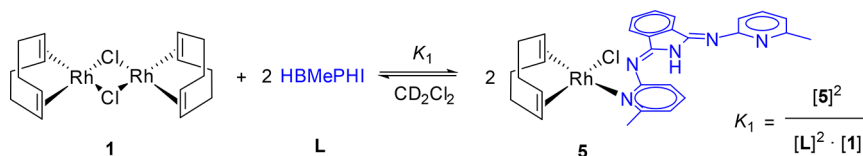
We are interested in developing catalysts for the dehydrogenation of hydrogen carriers,⁹ in particular those based on organic liquids.^{9f–h} Thus, in the search for new precursors, some years ago we initiated a research program based on platinum-group-metal complexes and the polynitrogenated organic molecule 1,3-bis(6'-methyl-2'-pyridylimino)-isoindoline (HBMePHI).¹⁰ Previously, with a few exceptions,¹¹ the anion of this isoindoline had been used as a pincer ligand, which modulates the electron density of the metal center and the steric hindrance around it.¹² However, it is much more than that. We have recently reported that platinum-group-metal polyhydride complexes promote the sequential activations of bonds N–H and C–H of the isoindoline core, to afford homobinuclear and heterobinuclear compounds via mononuclear intermediates (Scheme 1). The bonding of the second metal fragment modifies the electronic structure of the polydentate ligand, which produces a noticeable perturbation of the electron density around the initial center. As a consequence of the mutual electronic influence between the metals, catalytic synergism is observed in

the acceptorless and base-free dehydrogenation of secondary alcohols. The bridging ligand displays a noninnocent character, participating in the formation of the metal–alkoxide bond and in the release of molecular hydrogen.^{10b}

These unusual findings in the chemistry of pyridylimino-isoindolines prompted us to study the behavior of HBMePHI toward the dimers $[\text{M}(\mu\text{-Cl})(\eta^4\text{-C}_8\text{H}_{12})_2]$ ($\text{M} = \text{Rh}$ (1), Ir (2)) and $[\text{M}(\mu\text{-OH})(\eta^4\text{-C}_8\text{H}_{12})_2]$ ($\text{M} = \text{Rh}$ (3), Ir (4)), which are cornerstones in the development of rhodium¹³ and iridium¹⁴ organometallic chemistry. This paper reports the results of this study, including the formation of novel eight-membered heterodimetallacycles and C–N bond activations in the isoindoline core, some degradation pathways of the polydentate ligand in basic medium, and the catalytic ability of some of the new complexes in the acceptorless and base-free dehydrogenation of secondary alcohols.

RESULTS AND DISCUSSION

Reactions with 1 and 2. The addition of 2.0 mol of HBMePHI to dichloromethane- d_2 solutions of 1 (1.0 equiv per

Scheme 2. Formation of **5**

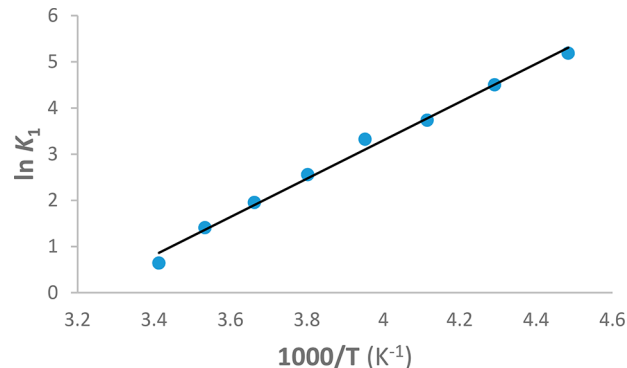
rhodium), contained in an NMR tube, produces a change in the solution color from yellow to orange. The ^1H NMR spectrum of the mixture at room temperature shows the resonances of **1** and HBMePHI (**L**), which appear slightly broadened, along with markedly broad signals corresponding to a new species. When the sample temperature is lowered, narrowing of all the signals is observed. At the same time, a decrease in the concentrations of both **1** and the isoidoline and an increase in the amount of a new species is clearly evident (Figure 1). Characteristic features of the new compound are 4 resonances between 4.6 and 3.3 ppm due to olefinic hydrogen atoms, which are all inequivalent, and 10 aromatic signals between 9.1 and 6.5 ppm corresponding to the CH hydrogen atoms of the coordinated ligand, which are also inequivalent. In agreement with the ^1H NMR spectrum, the $^{13}\text{C}\{^1\text{H}\}$ NMR spectrum at 213 K of the new complex displays 4 doublets ($J_{\text{C-Rh}} = 11\text{--}13$ Hz) between 82 and 74 ppm for the olefinic carbon atoms and 10 aromatic signals for the coordinated isoidoline. These observations can be rationalized according to the equilibrium shown in Scheme 2, which involves the formation of the mononuclear square-planar complex $\text{RhCl}(\eta^4\text{-C}_8\text{H}_{12})\{\kappa^1\text{-N}_{\text{py}}\text{-(HBMePHI)}\}$ (**5**), as a result of the rupture of the chloride bridges of **1** and the coordination of the polydentate molecule to the metal center by one of the pyridyl groups. The equilibrium was studied as a function of the temperature between 293 and 223 K by integration of the olefinic resonances and the higher field aromatic signal of the free ligand. Table 1 collects the values of

Table 1. Formation Constants K_1 and K_2 (L mol^{-1}) for **5** and **6**

temp (K)	K_1 (Scheme 2)	K_2 (Scheme 3)
293	1.897	
283	4.077	0.022
273	7.043	0.028
263	12.883	0.04
253	27.692	0.068
243	41.793	0.136
233	89.937	0.242
223	178.606	0.465
213		0.945
203		1.597
193		1.871
183		5.160

the equilibrium K_1 constants at each temperature. A linear least-squares analysis of $\ln K_1$ versus $1/T$ (Figure 2) provides values for ΔH° and ΔS° of -8.2 ± 0.3 kcal mol^{-1} and -26.4 ± 1.0 cal mol^{-1} K^{-1} , respectively.

The ^1H and $^{13}\text{C}\{^1\text{H}\}$ NMR spectra of the solutions resulting from the addition of 1.0 mol of HBMePHI per dimer to **1** in dichloromethane- d_2 show significant differences with regard to the previously mentioned spectra. Two noticeable features should be pointed out: the absence of resonances correspond-

Figure 2. van't Hoff plot for the equilibrium constant K_1 .

ing to the free ligand and the presence of signals due to a new compound. The latter is formed by the reaction of **1** with **5**, and its concentration increases as the sample temperature is decreased. **5** it has four inequivalent olefinic hydrogen atoms. Thus, its ^1H NMR spectra contain four resonances between 4.6 and 3.4 ppm. Nevertheless, these spectra only show three complex aromatic signals in the 8.2–6.9 ppm range. These observations are consistent with the formation of an equilibrium mixture among **1**, **5**, and the dimer $[\text{RhCl}(\eta^4\text{-C}_8\text{H}_{12})_2\{\mu\text{-N}_{\text{py}}\text{N}_{\text{py}}\text{-(HBMePHI)}\}]$ (**6** in Scheme 3). The $^{13}\text{C}\{^1\text{H}\}$ NMR spectra of the mixture are strong additional evidence in favor of this equilibrium. Figure 3 shows the $^{13}\text{C}\{^1\text{H}\}$ -APT spectrum in the olefinic region, at 183 K. The equilibrium shown in Scheme 3 was also studied as a function of the temperature between 283 and 183 K. The thermodynamic parameters obtained from the values of the equilibrium constant K_2 (Table 1) are $\Delta H^\circ = -5.8 \pm 0.2$ kcal mol^{-1} and $\Delta S^\circ = -28.0 \pm 0.7$ cal mol^{-1} K^{-1} (Figure 4).

The iridium dimer **2** also reacts with 1.0 and 0.5 equiv of HBMePHI. The reactions lead to the iridium counterparts of **5** and **6**. These complexes, $\text{IrCl}(\eta^4\text{-C}_8\text{H}_{12})\{\kappa^1\text{-N}_{\text{py}}\text{-(HBMePHI)}\}$ (**7**) and $[\text{IrCl}(\eta^4\text{-C}_8\text{H}_{12})_2\{\mu\text{-N}_{\text{py}}\text{N}_{\text{py}}\text{-(HBMePHI)}\}]$ (**8**), are significantly more stable than their rhodium analogues and can be isolated as pure red (**7**) and yellow (**8**) solids in 54% and 80% yields, respectively. The formation of the four compounds might take place via the intermediates $(\eta^4\text{-C}_8\text{H}_{12})\text{ClM}(\mu\text{-Cl})\text{M}\{\kappa^1\text{-N}_{\text{py}}\text{-(HBMePHI)}\}(\eta^4\text{-C}_8\text{H}_{12})$ ($\text{M} = \text{Rh}$ (**A**), Ir (**B**)), according to Scheme 4.

Complexes **7** and **8** were characterized by X-ray diffraction analyses. Figure 5 shows the structure of **7**, whereas Figure 6 gives a view of **8**. They confirm the selective coordination of the pyridyl groups of the polydentate HBMePHI molecule and the square-planar environment of the metal centers in these compounds. The coordination gives rise to Ir–N bonds of 2.124(4) Å (Ir–N(1); **7**) and 2.111(6) Å (Ir–N(1); **8**). These bond lengths compare well with those previously reported for other square-planar iridium(I) pyridine derivatives.¹⁵ The 1,5-cyclooctadiene ligand takes its customary “tub” conformation. The coordinated bonds display distances of 1.403(7) Å (C(21)–C(22)) and 1.428(7) Å (C(25)–C(26)) in **7** and

Scheme 3. Formation of 6

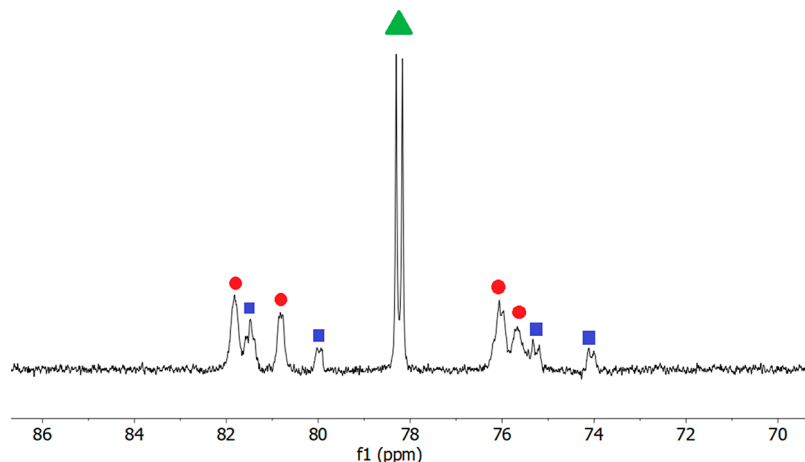
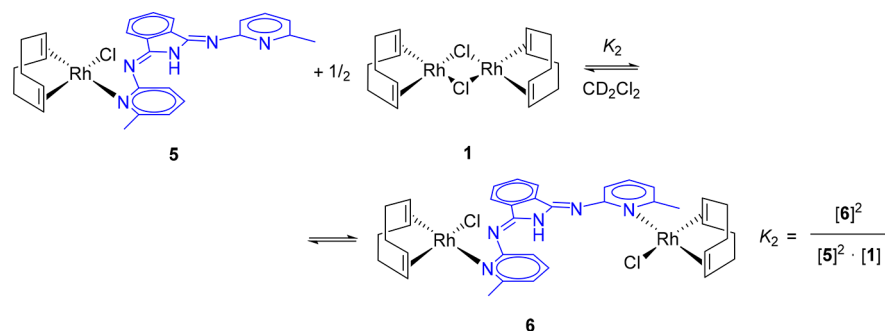


Figure 3. Olefinic resonances in the $^{13}\text{C}\{^1\text{H}\}$ NMR spectrum for the equilibrium shown in Scheme 3: blue ■, 5; green ▲, 1; red ●, 6 (183 K, 100.6 MHz, in CD_2Cl_2).

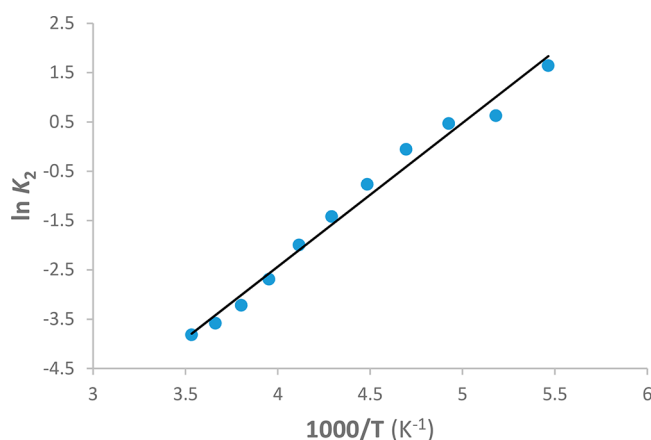


Figure 4. van't Hoff plot for the equilibrium constant K_2 .

1.413(11) Å (C(11)–C(12)) and 1.410(12) Å (C(15)–C(16)) in **8**, which are longer than the C–C double bonds in the free diolefin (1.34 Å) in agreement with the usual Chatt–Dewar–Duncanson model.¹⁶

Reactions with 3 and 4. In contrast to the chloride bridging ligand, one of the hydroxide groups of the rhodium dimer **3** is able to abstract the N–H hydrogen atom of HBMePHI. Thus, the treatment of yellow suspensions of this complex, in propan-2-ol, with 1.0 mol of the polydentate molecule for 2 h affords $[\text{Rh}(\eta^4\text{-C}_8\text{H}_{12})]_2(\mu\text{-OH})\{\mu\text{-}N_{\text{iso}}N_{\text{py}}\text{-}(\text{BMePHI})\}$ (**9**), as a consequence of the asymmetrical coordination of the resulting anion; one pyridyl group coordinates to a rhodium atom, whereas the other metal

center is bonded to the N atom of the isoindolate core. This coordination fashion and the remaining hydroxide group give rise to a mixed double bridge, which generates an eight-membered heterodimetallic cycle. Under the same conditions, complex **4** leads to the iridium counterpart $[\text{Ir}(\eta^4\text{-C}_8\text{H}_{12})]_2(\mu\text{-OH})\{\mu\text{-}N_{\text{iso}}N_{\text{py}}\text{-}(\text{BMePHI})\}$ (**10**). The formation of **9** and **10** should take place via the intermediates $(\eta^4\text{-C}_8\text{H}_{12})(\text{OH})\text{M}(\mu\text{-OH})\text{M}\{\kappa^1\text{-}N_{\text{py}}\text{-}(\text{HBMePHI})\}(\eta^4\text{-C}_8\text{H}_{12})$ (M = Rh (**C**), Ir (**D**)), the hydroxo counterparts of **A** and **B**, according to Scheme 5. Similarly to **1** and **2**, dimers **3** and **4** should initially undergo the rupture of a bridge, by coordination of a pyridyl group of HBMePHI to one of the metal centers. Thus, the subsequent heterolytic N–H activation of the isoindoline core by the other metal center, using the terminal hydroxide group as an internal base, would afford the mixed double bridge. Complexes **9** and **10** were isolated as orange solids in 80% and 47% yields, respectively.

The rhodium complex **9** was characterized by an X-ray diffraction analysis. The structure (Figure 7) proves the formation of the eight-membered heterodimetallic cycle, which displays a boat–boat conformation¹⁷ with the metals separated by 3.423 Å. The environment around each metal is square-planar, as expected for rhodium(I) centers. The Rh(1)–pyridine distance of 2.1495(14) Å (Rh(1)–N(1)) is about 0.05 Å longer than the Rh(2)–isoindoline bond length of 2.1047(14) Å (Rh(2)–N(3)), suggesting a higher nucleophilicity for the isoindoline N(3) atom than for the pyridine N(1) atom. As a consequence of this, the Rh(1)–hydroxide bond of 2.0709(12) Å (Rh(1)–O(1)) is about 0.02 Å shorter than the Rh(2)–hydroxide bond of 2.0912(12) Å (Rh(2)–O(1)). The

Scheme 4. Formation of Complexes 5–8

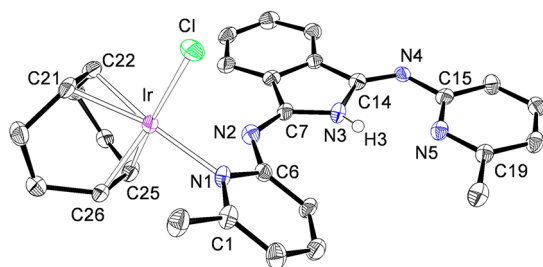
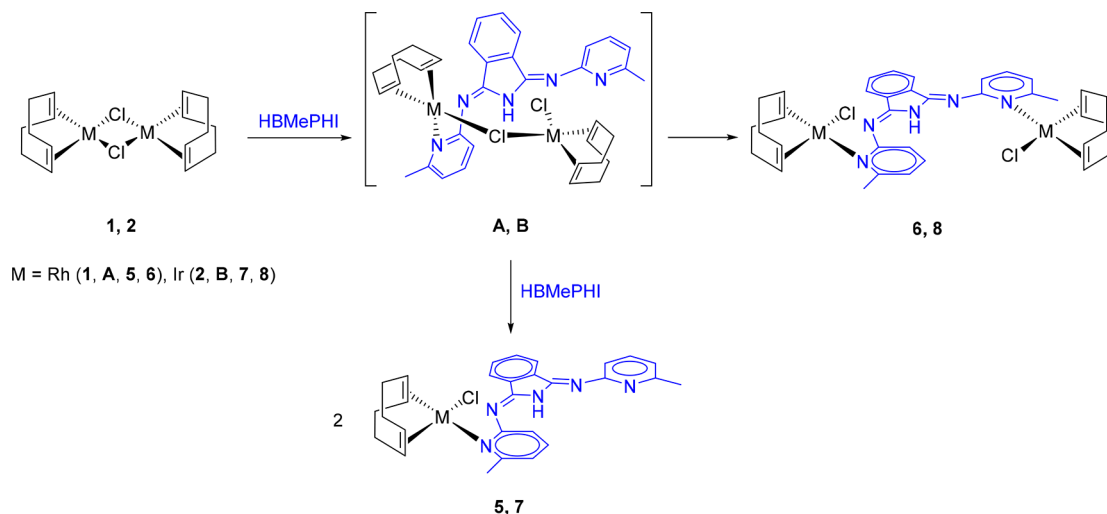


Figure 5. Molecular diagram of complex 7 (50% probability ellipsoids). Hydrogen atoms (except H(3)) are omitted for clarity. Selected bond lengths (Å): Ir–Cl = 2.3608(13), Ir–N(1) = 2.124(4), Ir–C(21) = 2.099(4), Ir–C(22) = 2.112(5), Ir–C(25) = 2.109(5), Ir–C(26) = 2.096(5), N(1)–C(1) = 1.356(6), N(1)–C(6) = 1.368(5), N(2)–C(6) = 1.381(6), N(3)–C(7) = 1.377(6), N(3)–C(14) = 1.400(6), C(21)–C(22) = 1.403(7), C(25)–C(26) = 1.428(7).

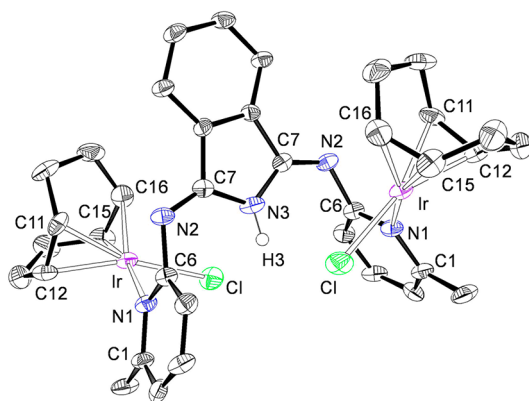


Figure 6. Molecular diagram of complex 8 (50% probability ellipsoids). Hydrogen atoms (except H(3)) are omitted for clarity. Selected bond lengths (Å): Ir–Cl = 2.360(2), Ir–N(1) = 2.111(6), Ir–C(11) = 2.120(7), Ir–C(12) = 2.089(9), Ir–C(15) = 2.137(8), Ir–C(16) = 2.116(8), N(1)–C(6) = 1.338(9), N(2)–C(6) = 1.438(9), N(2)–C(7) = 1.276(9), N(3)–C(7) = 1.386(8), C(11)–C(12) = 1.413(11), C(15)–C(16) = 1.410(12).

lengths of the coordinated C–C double bonds to both metal centers are similar, between 1.393(3) and 1.403(3) Å, and compare well with the distances found in 7 and 8. Several

conformations of similar energy are possible for an eight-membered cycle. As a consequence, complexes 9 and 10 are fluxional in toluene-*d*₈ solution, showing a rigid structure at temperatures lower than 213 K. In agreement with Figure 7, their ¹H NMR spectra display eight olefinic resonances between 5.5 and 3.0 ppm, whereas the ¹³C{¹H} NMR spectra contain eight olefinic signals in the 85–52 ppm range.

The chelate κ^2 -(*N*_{iso},*N*_{py}) coordination is known for 1,3-bis(2'-pyridylimino)isoindolate (BPHI) anions.¹¹ However, as far as we know, the bridge μ -(*N*_{iso},*N*_{py}) coordination is unprecedented. Compounds bearing bridging [BPHI][−] ligands are very scarce. Baird and co-workers have observed that HBPHI displaces an acetate group from Mo₂(OAc)₄ to give Mo₂(OAc)₃(BPHI), with the [BPHI][−] ligand bound to one molybdenum by an imino nitrogen and to the other molybdenum by the isoindoline nitrogen and a pyridyl nitrogen.¹⁸ Bröring and co-workers have reported that one of the pyridyl groups of HBMePHI undergoes a palladium-promoted 1,3-hydrogen shift, from C to N, to afford Pd(κ^3 -*N*_{py},*N*_{iso},*C*_{Hpy})-pincer derivatives, which add a second palladium to the free pyridyl-imine moiety.¹⁹ We have described the preparation of homoleptic and heteroleptic bis(osmium) complexes containing a [μ -(κ^2 -*N*_{py},*N*_{imine})₂-BMePHI][−] ligand,^{10a} whereas Li, Yang, Zhang, and co-workers have observed the same coordination fashion in an intermediate species formed in the reaction of Lu(CH₂SiMe₃)₃(thf)₂ with HBPHI to give Lu{ κ^3 -*mer*-(BPHI)}(CH₂SiMe₃)₂.²⁰

Degradation of the [BMePHI][−] ligand in Basic Medium. Alcohol dehydrogenation catalysts combined with bases promote borrowing-hydrogen reactions, including α -alkylation of arylacetonitriles and methyl ketones.²¹ The carbonyl compound resulting from the dehydrogenation process undergoes a base-catalyzed condensation with an alkyl substrate to afford an α,β -unsaturated intermediate,²² which is subsequently reduced to the final product with the hydrogen generated in the dehydrogenation.²¹ In order to explore the ability of the Rh- and Ir(BMePHI)(diolefin) systems to work in this class of catalysis, we studied the formation of 9 and 10 in the presence of a strong base.

Treatment of a suspension of 3 in propan-2-ol with 2.0 mol of HBMePHI and 3.0 equiv of KO^tBu at room temperature for 2 h leads to a mixture of 9 and [Rh(η^4 -C₈H₁₂)₂]₂{ μ -*N*_{iso},*N*_{imine}-

Scheme 5. Formation of 9 and 10

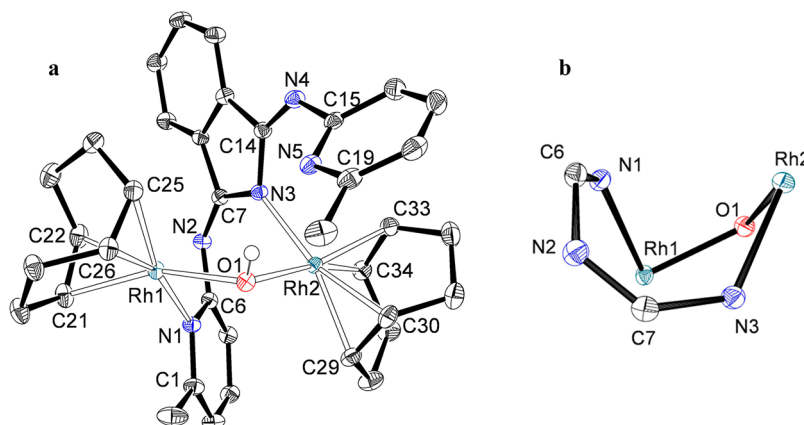
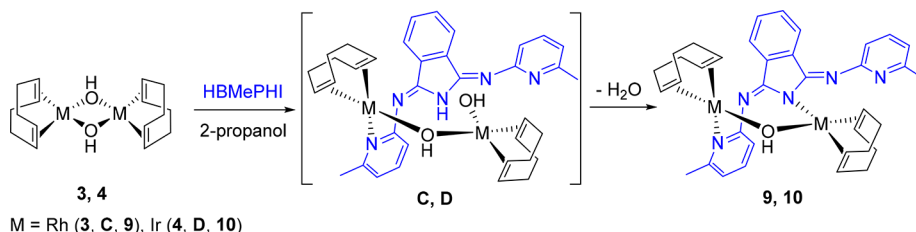
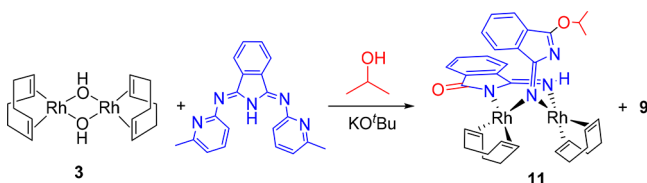


Figure 7. (a) Molecular diagram of complex **9** (50% probability ellipsoids). All hydrogen atoms (except that of the hydroxide ligand) are omitted for clarity. Selected bond lengths (Å) and angles (deg): Rh(1)–O(1) = 2.0709(12), Rh(2)–O(1) = 2.0912(12), Rh(1)–N(1) = 2.1495(14), Rh(2)–N(3) = 2.1047(14), Rh(1)–C(21) = 2.1016(18), Rh(1)–C(22) = 2.1155(18), Rh(1)–C(25) = 2.1075(17), Rh(1)–C(26) = 2.1096(17), N(1)–C(6) = 1.357(2), N(2)–C(6) = 1.382(2), N(2)–C(7) = 1.288(2), N(3)–C(7) = 1.388(2), N(3)–C(14) = 1.391(2), N(4)–C(14) = 1.287(2), N(4)–C(15) = 1.391(2), Rh(1)–O(1)–Rh(2) = 110.63(6), O(1)–Rh(1)–N(1) = 86.48(5), O(1)–Rh(2)–N(3) = 87.63(5). (b) Molecular core.

(HN=C₈H₄NO)}(μ-N=C₈H₄NOⁱPr) (**11**), according to Scheme 6.

Scheme 6. Formation of 11



Complexes **9** and **11** were separated by using their different solubilities in propan-2-ol. Thus, complex **11** was obtained pure in 20% yield with regard to **3** as red crystals suitable for X-ray diffraction analysis. Its structure (Figure 8) reveals the formation of a surprising mixed double bridge. One of the halves of the bridge is the anion resulting from the deprotonation of the NH-isoindoline group of 3-iminoisoindolin-1-one (HN=C₈H₄NHO[−]), which coordinates different metal centers in an *N*_{iso}*N*_{imine} fashion, whereas the other half is the azavinylidene resulting from the deprotonation of the NH-imine unit of 3-isopropoxy-1*H*-isoindol-1-imine (HN=C₈H₄NOⁱPr). The formation of the [HN=C₈H₄NO][−] anion involves two different alcoholysis processes in the imine moieties of a [BMePHI][−] ligand. The C=O double bond could be the result of the substitution of a pyridylimine moiety by two isopropoxide groups. Then, the resulting diisopropylacetal intermediate²³ should lose diisopropyl ether to afford the carbonyl group.²⁴ In contrast, the other imino group undergoes alcoholysis of the imine–pyridyl bond. The

azavinylidene bridge ([N=C₈H₄NOⁱPr][−]) arises from a similar process involving two alcoholyses on the imine functions of a second [BMePHI][−] ligand. The main difference between the generation processes of both bridges is the number of molecules of propan-2-ol attacking the imine–isoindoline bond. When only a molecule of propan-2-ol attacks, the isopropoxide group remains as a substituent at the 2-position of the isoindoline core. Its steric hindrance prevents the coordination of the isoindoline-N atom, whereas the electronic difference with the carbonyl oxygen atom seems to favor the deprotonation of the imine resulting from the alcoholysis of the imine–pyridyl bond.

The rhodium atoms display square-planar coordination environments with a separation between the metals of 3.0672(5) Å, which is long for a single Rh–Rh bond. In agreement with this, overlap between their *d*_z² orbitals has not been found by means of DFT calculations (M06/6-311G(d,p) & SDD(f)). Although the isoindoline coordination of the anion [HN=C₈H₄NO][−] to Rh(1) of 2.090(3) Å (Rh(1)–N(3)) is about 0.01 Å shorter than the imine coordination to Rh(2) of 2.106(4) Å (Rh(2)–N(4)), the azavinylidene–rhodium bond lengths of 2.048(3) Å (Rh(1)–N(1)) and 2.049(3) Å (Rh(2)–N(1)) are statistically identical and similar to those reported for the complex [Rh(μ-N=CPh₂)(TFB)]₂ (TFB = tetrafluorobenzobarrelene; 2.046(7), 2.052(7), 2.054(6) and 2.054(7) Å).²⁵ The M–azavinylidene–M angle, Rh(1)–N(1)–Rh(2), of 96.93(14)° and the distance N(1)–C(1) of 1.260(5) Å compare well with those found in other transition-metal compounds bearing azavinylidene bridges.²⁶ The lengths of the coordinated C=C double bonds, between 1.353(8) and 1.387(7) Å, are slightly shorter than those found in **7** and **8**.

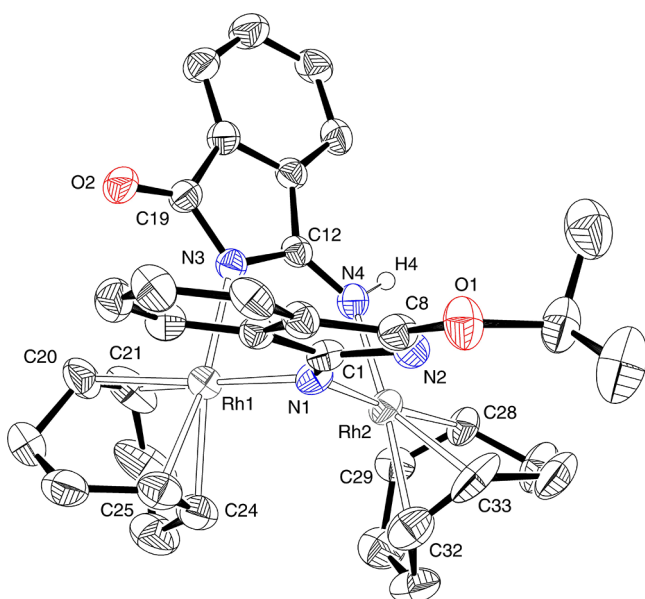


Figure 8. Molecular diagram of complex **11** (50% probability ellipsoids). All hydrogen atoms (except the imine hydrogen atom H4) are omitted for clarity. Selected bond lengths (Å) and angles (deg): Rh(1)–N(1) = 2.048(3), Rh(1)–N(3) = 2.090(3), Rh(2)–N(1) = 2.049(3), Rh(2)–N(4) = 2.106(4), Rh(1)–C(20) = 2.134(5), Rh(1)–C(21) = 2.125(5), Rh(1)–C(24) = 2.147(5), Rh(1)–C(25) = 2.125(5), Rh(2)–C(28) = 2.155(4), Rh(2)–C(29) = 2.115(5), Rh(2)–C(32) = 2.160(5), Rh(2)–C(33) = 2.106(5), N(1)–C(1) = 1.260(5), N(2)–C(1) = 1.449(5), N(2)–C(8) = 1.286(5), N(3)–C(12) = 1.364(5), N(3)–C(19) = 1.371(5), N(4)–C(12) = 1.292(5), O(1)–C(8) = 1.334(5), O(1)–C(9) = 1.471(5), O(2)–C(19) = 1.236(5). Rh(1)–N(1)–Rh(2) = 96.93(14).

The ^1H and $^{13}\text{C}\{^1\text{H}\}$ NMR spectra of **11** in benzene- d_6 at room temperature are consistent with the structure shown in Figure 8. The ^1H NMR spectrum displays a broad signal at 5.78 ppm corresponding to the imine-NH hydrogen atom and eight olefinic resonances due to the inequivalent $\text{C}_{\text{sp}^2}\text{-H}$ hydrogen atoms of the diene, between 6.5 and 3.3 ppm, whereas the $^{13}\text{C}\{^1\text{H}\}$ NMR spectrum contains eight doublets ($J_{\text{C-Rh}} = 10\text{--}13$ Hz) between 87 and 74 ppm, assigned to the coordinated carbon atoms.

The study of the electrochemistry of binuclear complexes is always attractive due to the possible interaction between the two metals. Unfortunately, complexes **9** and **10** were unstable and decomposed in the electrode, but the cyclic voltammetry of **11** was conducted under an argon atmosphere in dry, oxygen-free dichloromethane (10^{-3} M analyte concentration) containing $[\text{N}^n\text{Bu}_4]\text{PF}_6$ as the supporting electrolyte (10^{-1} M) and using a Ag/AgCl reference electrode (3 M, KCl). Under these conditions complex **11** displays two oxidation events, one of them quasi-reversible at 0.49 V and the second one irreversible at 1.10 V (Table 2 and Figures S1–S3). The DFT (M06/6-311G(d,p)&SDD(f)) calculations reveal that the HOMO of the complex is equally distributed between the metal centers, whereas the LUMO is located in the isindolinate $[\text{HN}=\text{C}_8\text{H}_4\text{NO}]^-$ ligand. The loss of one electron by each metal (two electrons per molecule) leads to the dication $[\mathbf{11}]^{2+}$, which also has the HOMO mainly centered on the metals, although some participation of the coordinated isindolinate anion is observed. The subsequent loss of two electrons affords the tetracation $[\mathbf{11}]^{4+}$, having the HOMO mainly centered on the isindolinate ligand (Figure

Table 2. Oxidation Potentials of Complexes **11** and **12**^a

complex	E_{pa1}	E_{pa2}	E_{pa3}
11	0.49 ^b (E_{pc1} 0.39) (ΔE 95 mV)	1.10	
12	0.56	0.74	1.37

^aData obtained from dichloromethane solutions of **11** and **12** (10^{-3} M), containing $(\text{NBu}_4)\text{PF}_6$ (10^{-1} M) as the supporting electrolyte at 20 °C: counter electrode, Pt; working electrode, glassy carbon; reference electrode, Ag/AgCl; scan rate, 100 mV/s. Values are given in V and referenced vs Ag/AgCl. ^bQuasi-reversible wave.

9). These data suggest that the oxidation events are compatible with two sequential processes of two electrons: from $\text{Rh}^{\text{II}}\text{L}_2\text{Rh}^{\text{II}}$

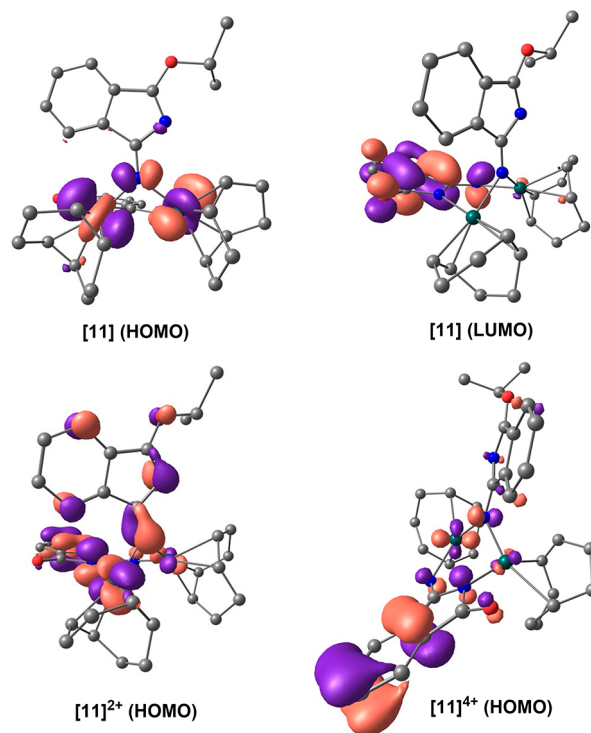
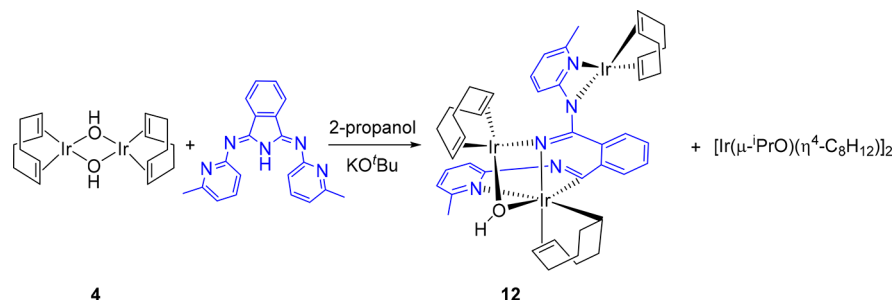


Figure 9. Computed (DFT/M06/6-311G(d,p)&SDD(f)) HOMO and LUMO orbitals for complex **11** and for the oxidation products dication $[\mathbf{11}]^{2+}$ and tetracation $[\mathbf{11}]^{4+}$. Hydrogen atoms are omitted for clarity. The isosurface value is 0.043.

to $\text{Rh}^{\text{III}}\text{L}_2\text{Rh}^{\text{II}}$ and from $\text{Rh}^{\text{III}}\text{L}_2\text{Rh}^{\text{II}}$ to $\text{Rh}^{\text{III}}\text{L}_2\text{Rh}^{\text{III}}$. The successive oxidations give rise to the approach of the metal centers to 2.780 Å in the dication and to 2.747 Å in the tetracation (Figure S6). Although these distances lie within the range of distances assumed for a Rh–Rh single bond (2.62–2.84 Å),²⁷ overlapping between the d orbitals of the metals is not observed.

The $\text{Ir}(\text{BMePHI})(\text{diolefin})$ systems are also unstable in basic medium. As in the rhodium case, the instability is associated with the reactivity of the $[\text{BMePHI}]^-$ ligand in basic medium, which is strongly directed by the metal center. Under the same conditions as those giving rise to the mixture of **9** and **11**, dimer **4** affords a mixture of the isopropoxide dimer $[\text{Ir}(\mu\text{-O}^i\text{Pr})(\eta^4\text{-C}_8\text{H}_{12})_2]_2$ and the trinuclear derivative $\text{Ir}_3(\eta^4\text{-C}_8\text{H}_{12})_2(\kappa^1\text{-C},\eta^2\text{-C}_8\text{H}_{13})(\mu\text{-OH})(\text{L})$ (**12** in Scheme 7). Using complex **10** as a reference, the L ligand of **12** can be described as the result of the oxidative addition of the C–N bond, substituted with the free pyridyl-imine group, of the five-membered ring of the isindoline core to the pyridyl-

Scheme 7. Formation of 12

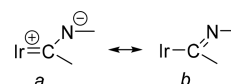


coordinated metal center. The addition of a hydride to one of the C–C double bonds of the diene coordinated to the generated iridium(III) center and the addition of an $[\text{Ir}(\eta^4\text{-C}_8\text{H}_{12})]^+$ fragment to the free pyridyl-imine group give rise to this novel molecule. The metal-promoted degradation of the five-membered heterocycle of an isindoline is certainly notable. In this context, it should be highlighted that the isindoline skeleton is a part of a large variety of biologically active synthetic compounds, which have a wide range of applications in medicine.²⁸

Complex 12 was separated from the mixture by extraction in toluene and crystallized pure in 22% yield with regard to 4 as orange crystals suitable for X-ray diffraction analysis. Its structure (Figure 10) proves the degradation of the

$[\text{BMePHI}]^-$ ligand and the trinuclear nature of the complex, which is formed by an octahedral iridium(III) center (Ir(1)) and two square-planar iridium(I) centers (Ir(2) and Ir(3)). The octahedron around Ir(1) is defined by two chelates and a hydroxide-azavinylidene double bridge. The chelate C_8H_{13} -carbocycle coordinates with three different Ir–C distances, as expected for the $\kappa^1\text{-C}, \eta^2$ -coordination, which compare well with those reported for other complexes bearing $\text{C}_8\text{H}_{12}\text{R}$ rings similarly linked to iridium(III).²⁹ The $\sigma\text{-Ir(1)–C(21)}$ single bond of 2.102(5) Å is about 0.06 and 0.07 Å shorter than the metal–olefin bonds Ir(1)–C(25) and Ir(1)–C(26) of 2.163(4) and 2.172(5) Å, respectively. The Ir(1)–C(21) bond is disposed *trans* to the pyridyl group of a (C(7),N(1))-iminyl-pyridine moiety (C(21)–Ir(1)–N(1) = 169.13(15)°), which has a N(1)–Ir(1)–C(7) bite angle of 74.85(15)°. The iridium–pyridine distance of 2.236(4) Å (Ir(1)–N(1)) is slightly longer than those found in 7 and 8, whereas the Ir(1)–C(7) bond length of 1.982(4) Å is about 0.02 Å shorter than the Ir(1)–C(21) single bond and even shorter than those reported for other iridium-iminyl derivatives.³⁰ This suggests that, for an adequate description of the Ir(1)–C(7) bonding situation, the resonance form *a* shown in Chart 1 should also

Chart 1. Resonance for the Ir(1)–C(7) Bond



be taken into account. Atom C(7) is disposed *trans* to the hydroxide group with a C(7)–Ir(1)–O(1) angle of 151.58(14)°, while the other part of the double bridge, the azavinylidene ligand, lies *trans* to the C(25)–C(26) double bond. The double bridge and the Ir(2) atom form a metalloligand, which coordinates to Ir(1) with an O(1)–Ir(1)–N(3) bite angle of 73.32(12)°. The iridium–azavinylidene distances of 2.047(3) Å (Ir(1)–N(3)) and 2.035(3) Å (Ir(2)–N(3)) are statistically identical. However, the Ir(1)–O(1) distance of 2.253(3) Å is about 0.17 Å longer than the Ir(2)–O(1) bond length of 2.072(3) Å. The $N_{\text{imine}}N_{\text{py}}$ chelate coordinates to Ir(3) with a N(4)–Ir(3)–N(5) bite angle of 63.61(13)°, which compares well with the reported angles for the $\kappa^2\text{-N}_{\text{py}}, N_{\text{imine}}$ -coordination of the $[\text{BMePHI}]^-$ anion.¹⁰ The coordinated C=C double bonds display distances between 1.299(6) and 1.429(6) Å. The asymmetry of 12 is also evident in the ^1H and $^{13}\text{C}\{^1\text{H}\}$ NMR spectra. Thus, the former shows 10 olefinic resonances between 5.6 and 3.0 ppm, due to the inequivalent $\text{C}_{\text{sp}^2}\text{H}$ -hydrogen atoms of the carbocycles, in addition to the signals corresponding to the Ir(1)C(21)H- and OH-hydrogen atoms, which appear at 0.65 and 0.24 ppm, respectively. The $^{13}\text{C}\{^1\text{H}\}$ NMR spectrum agrees with the ^1H

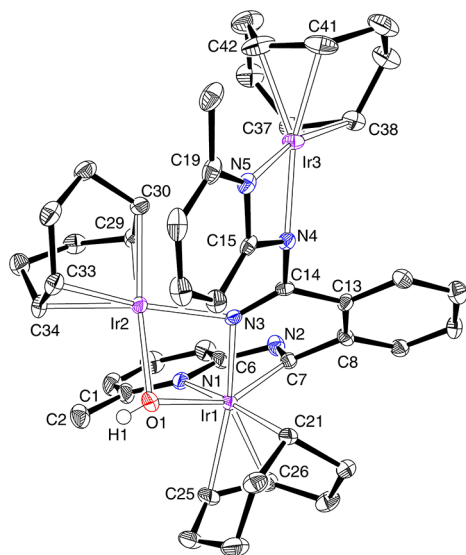


Figure 10. Molecular diagram of complex 12 (50% probability ellipsoids). All hydrogen atoms (except that of the hydroxide ligand) are omitted for clarity. Selected bond lengths (Å) and angles (deg): Ir(1)–C(7) = 1.982(4), Ir(1)–N(3) = 2.047(3), Ir(1)–N(1) = 2.236(4), Ir(1)–O(1) = 2.253(3), Ir(1)–C(21) = 2.102(5), Ir(1)–C(25) = 2.163(4), Ir(1)–C(26) = 2.172(5), Ir(2)–N(3) = 2.035(3), Ir(2)–O(1) = 2.072(3), Ir(2)–C(29) = 2.071(4), Ir(2)–C(30) = 2.120(4), Ir(2)–C(33) = 2.101(4), Ir(2)–C(34) = 2.130(4), Ir(3)–N(4) = 2.072(3), Ir(3)–C(37) = 2.096(4), Ir(3)–C(38) = 2.111(5), Ir(3)–C(41) = 2.114(5), Ir(3)–C(42) = 2.092(5), N(1)–C(1) = 1.367(5), N(1)–C(6) = 1.370(5), N(2)–C(6) = 1.396(5), N(2)–C(7) = 1.301(5), N(3)–C(14) = 1.296(5), N(4)–C(14) = 1.403(5), N(4)–C(15) = 1.379(5), N(5)–C(15) = 1.357(5), N(5)–C(19) = 1.357(5), C(21)–Ir(1)–N(1) = 169.13(15), N(1)–Ir(1)–C(7) = 74.85(15), C(7)–Ir(1)–O(1) = 151.58(14), O(1)–Ir(1)–N(3) = 73.32(12), N(4)–Ir(3)–N(5) = 63.61(13).

NMR spectrum. Thus, it contains 10 olefinic resonances between 86.5 and 32.3 ppm. The signal corresponding to the carbocyclic C(21) atom is observed at 32.1 ppm, whereas that due to the iminyl C(7) atom appears at 198.9 ppm. This chemical shift, at an unusually low field, is more evidence for a significant contribution of the resonance form *a* to the Ir(1)–C(7) bond.

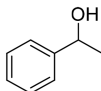
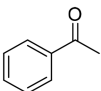
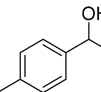
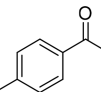
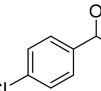
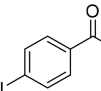
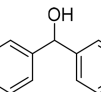
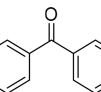
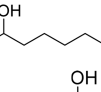
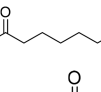
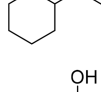
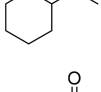
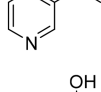
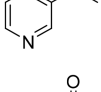
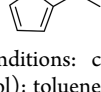
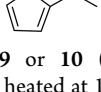
The electrochemical behavior of binuclear complex **12** is summarized in Table 2. As shown in Figures S4 and S5, it undergoes three irreversible oxidations at 0.56, 0.74, and 1.37 V. The DFT (M06/6-311G(d,p)&SDD(f)) calculations reveal that the HOMO of the molecule is mainly located on the iridium(I) center Ir(2), whereas the LUMO is distributed along the octahedral iridium(III) center Ir(1) and its associated ligands (Figures S7–S9). After the loss of one electron, the spin density of the molecule is still localized on Ir(2) (computed spin density 0.71 e[−]). Thus, it is reasonable to think that the second oxidation also takes place on this center. Thus, the peaks at 0.56 and 0.74 V can be assigned to the sequential oxidations of Ir(2), from Ir(I) to Ir(II) and from Ir(II) to Ir(III). It is likely that the third oxidation at 1.37 V could correspond to the other iridium(I) center, Ir(3). Overall, the oxidation of **12** is mainly determined by the oxidation states of the metal centers, which behave independently from each other.

Acceptorless and Base-Free Dehydrogenation of Secondary Alcohols Catalyzed by **9 and **10**.** The reactions were performed in toluene at 100 °C, using a substrate concentration of 0.255 M and a catalyst concentration of 9.0×10^{-3} M (i.e., 7 mol % of the metal). Table 3 collects the alcohols studied and the yield of carbonyl compounds formed as a function of the catalyst after 24 h.

Ketones are obtained in moderate to high yields after 24 h. Both catalysts are more efficient for the dehydrogenation of aliphatic alcohols in comparison to that for benzylic or benzhydrylic alcohols. Thus, while ketones resulting from the dehydrogenation of substrates such as 1-phenylethanol, 3-pyridylethanol, 1-(2-furyl)ethanol, and diphenylmethanol are obtained in 20–60% yield, 2-octanol and 1-cyclohexylethanol are dehydrogenated in about 70% yield. Complexes **9** and **10** are even more efficient than the binuclear polyhydrides shown in Scheme 1, (PⁱPr₃)₂H₂Ir{μ-(κ²-N_{py},N_{imine}-BMePI-κ²-N_{imine},C⁴_{iso})}IrH₂(PⁱPr₃)₂ and (PⁱPr₃)₂H₂Ir{μ-(κ²-N_{py},N_{imine}-BMePI-κ²-N_{imine},C⁴_{iso})}OsH₃(PⁱPr₃)₂, for the dehydrogenation of aliphatic alcohols.^{10b} This ability is in contrast to the generally observed trend. Aromatic groups stabilize the ketone and appear to increase the dehydrogenation rate of the alcohol. The rhodium complex **9** is significantly more efficient than the iridium derivative **10** for the dehydrogenation of aromatic substrates, in particular for 3-pyridylethanol, 1-(2-furyl)ethanol, and diphenylmethanol, whereas the oxidation of aliphatic alcohols occurs with similar efficiency in the presence of both complexes.

The catalysis can be rationalized according to Scheme 8. The alcohol, which is in great excess with regard to the metal complexes, should initially displace the bridging hydroxide ligand to afford the related alkoxide derivatives [M(η⁴-C₈H₁₂)]₂(μ-OCHR'R'){μ-N_{iso},N_{py}-(BMePI)} (E), which would be the catalytically active species of the dehydrogenation process. As in the reactions catalyzed by the polyhydrides shown in Scheme 1,¹⁰ the addition of the O–H bond of the alcohols to the bond M–N_{iso} of E could generate the intermediates (η⁴-C₈H₁₂)(R'R'CHO)M(μ-OCHR'R')M{κ¹-

Table 3. Metal-Mediated Acceptorless and Base-Free Dehydrogenation of a Secondary Alcohol^a

Substrate	Product	Yield(%) with 9	Yield(%) with 10
		48	46
		60	49
		54	29
		60	39
		71	69
		70	69
		42	19
		30	17

^aConditions: complex **9** or **10** (0.009 mmol); substrate (0.255 mmol); toluene (1 mL); heated at 100 °C for 24 h. Conversions were calculated from the relative peak area integrations of the reactant and product in the GC spectra.

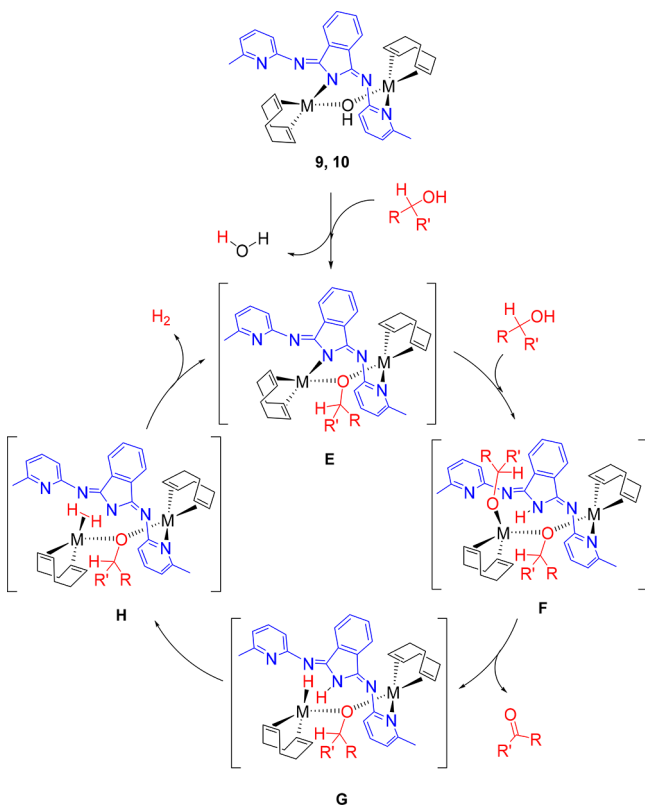
N_{py}-(HBMePHI)}(η⁴-C₈H₁₂) (F), the alkoxide counterparts of A–D. Then, the subsequent β-hydrogen elimination on the terminal alkoxide group could afford the ketone and the hydride species (η⁴-C₈H₁₂)HM(μ-OCHR'R')M{κ¹-N_{py}-(HBMePHI)}(η⁴-C₈H₁₂) (G), which would evolve into (η⁴-C₈H₁₂)(η²-H₂)M(μ-OCHR'R')M{κ¹-N_{py}-(HBMePHI)}(η⁴-C₈H₁₂) (H) via heterolytic H–H formation.³¹ The subsequent substitution of the dihydrogen ligand by the isoindoline-N atom should release molecular hydrogen, regenerating the active species E.

The cycle shown in Scheme 8 is consistent with those proposed for the dehydrogenations promoted by the polyhydrides of Scheme 1. The noninnocent character of the bridging ligand is shown by the addition of the O–H bond of the alcohol to the M–N_{iso} bond of E and in the formation of H. However, in this case, only a metal center would have a direct participation in the catalysis. The function of the other should be to keep the isoindoline N–H bond in the proximity of the active center.

CONCLUDING REMARKS

This study has revealed that a pyridyl group of 1,3-bis(6'-methyl-2'-pyridylimino)isoindoline (HBMePHI) coordinates

Scheme 8. Catalytic Cycle for the Acceptorless and Base-Free Dehydrogenation of Secondary Alcohols Promoted by Complexes 9 and 10



to a metal center of the dimers $[M(\mu-X)(\eta^4-C_8H_{12})]_2$ ($M = \text{Rh, Ir}$; $X = \text{Cl, OH}$) to afford square-planar species, splitting at least one of the bridges. The subsequent deprotonation of the N–H bond of the isoindoline core by a hydroxo group leads to the complexes $[M(\eta^4-C_8H_{12})]_2(\mu-OH)\{\mu-N_{iso}, N_{py}-(\text{BMePHI})\}$ ($M = \text{Rh, Ir}$), which are efficient catalyst precursors for the acceptorless and base-free dehydrogenation of secondary alcohols. These compounds cannot be used in catalytic processes needing a basic medium, because the $[\text{BMePHI}]^-$ ligand undergoes degradation. Depending upon the metal center of the complex, three different deteriorations have been observed: (i) alcoholysis of an exocyclic isoindoline–N double bond, (ii) alcoholysis of a N-pyridyl bond, and (iii) opening of the five-membered ring of the isoindoline core by oxidative addition of one of the C–N bonds to a metal center of the catalyst precursor.

In summary, 1,3-bis(2'-pyridylimino)isoindolinates are interesting organic anions, which can act as noninnocent bridging ligands in diverse catalysts for the acceptorless and base-free dehydrogenation of secondary alcohols. However, they should be not employed to stabilize catalysts of processes which take place in basic media, since they undergo degradation.

EXPERIMENTAL SECTION

All reactions were carried out with rigorous exclusion of air using Schlenk-tube techniques. Solvents were dried using standard procedures and distilled under an argon atmosphere or obtained dry from an MBraun solvent purification apparatus. ^1H and $^{13}\text{C}\{^1\text{H}\}$ NMR spectra (Figures S10–S30) were recorded on a Bruker Avance 300 MHz, Bruker Avance 400 MHz, or Bruker Avance 500 MHz

instrument. Chemical shifts (expressed in ppm) are referenced to residual solvent peaks (^1H , $^{13}\text{C}\{^1\text{H}\}$). Coupling constants J are given in hertz. C, H, and N analyses were carried out with a PerkinElmer 2400 CHNS/O analyzer or with a Thermo FlashEA 1112 CHNS/O analyzer. High-resolution electrospray mass spectra (HRMS) were acquired using a MicroTOF-Q hybrid quadrupole time-of-flight spectrometer (Bruker Daltonics, Bremen, Germany). $[\text{Rh}(\mu\text{-Cl})(\eta^4-C_8H_{12})]_2$ (1),³² $[\text{Ir}(\mu\text{-Cl})(\eta^4-C_8H_{12})]_2$ (2),³³ $[\text{Rh}(\mu\text{-OH})(\eta^4-C_8H_{12})]_2$ (3),³⁴ $[\text{Ir}(\mu\text{-OH})(\eta^4-C_8H_{12})]_2$ (4),³⁵ and 1,3-bis(6'-methyl-2'-pyridylimino)isoindoline (HBMePHI)³⁶ were prepared according to the published methods.

General Procedure for the Rh- and Ir-Catalyzed Dehydrogenation Reactions of Alcohols. A solution of the catalyst (9 or 10, 0.009 mmol) and the corresponding substrate (0.255 mmol) in toluene (1 mL) was placed in a Schlenk flask equipped with a condenser under an argon atmosphere. The mixture was stirred at 100 °C for 24 h. After this time the solution was cooled to room temperature, and the progress of the reaction was monitored by GC (Agilent 6890N gas chromatograph with a flame ionization detector, using an Agilent 19091N-133 polyethylene glycol column (30 m \times 250 μm \times 0.25 μm thickness)). The oven conditions used are as follows: 80 °C (hold 5 min) to 200 °C at 15 °C/min (hold 7 min), except for diphenylmethanol, 150 °C (hold 5 min) to 240 °C at 15 °C/min (hold 13 min). The obtained values of the yield are the average of two runs. The identity of the compound was confirmed by comparison of the retention time of the product.

Addition of 2.0 mol of HBMePHI to $[\text{Rh}(\mu\text{-Cl})(\eta^4-C_8H_{12})]_2$ (1). At room temperature, 19 mg (0.06 mmol) of HBMePHI was added to 0.5 mL of a dichloromethane- d_2 solution of 1 (15 mg, 0.03 mmol) in an NMR tube. After 10 min, ^1H NMR spectra between 293 and 223 K (Figure 1) and the $^{13}\text{C}\{^1\text{H}\}$ NMR spectrum at 213 K (Figure S12) were recorded. HRMS (electrospray, m/z): calcd for $\text{C}_{28}\text{H}_{29}\text{RhN}_5\text{ClNa}$ [$M + \text{Na}$]⁺ 596.1059, found 596.1038. Selected spectroscopic data for $\text{RhCl}(\eta^4-C_8H_{12})\{\kappa^1-N_{py}-(\text{HBMePHI})\}$ (5) are as follows. ^1H NMR (400 MHz, CD_2Cl_2 , 223 K): δ 12.70 (s, 1H, NH), 8.91 (d, $^3J_{\text{H-H}} = 7.4$, 1H, CH_{arom}), 8.04 (dt, $^3J_{\text{H-H}} = 7.4$, $^3J_{\text{H-H}} = 1.0$, 1H, CH_{arom}), 7.86 (td, $^3J_{\text{H-H}} = 7.5$, $^3J_{\text{H-H}} = 1.2$, 1H, CH_{arom}), 7.80 (td, $^3J_{\text{H-H}} = 7.5$, $^3J_{\text{H-H}} = 1.2$, 1H, CH_{arom}), 7.74 (t, $^3J_{\text{H-H}} = 7.8$, 1H, CH_{arom}), 7.63 (t, $^3J_{\text{H-H}} = 7.6$, 1H, CH_{arom}), 7.25 (d, $^3J_{\text{H-H}} = 7.9$, 1H, CH_{arom}), 7.21 (d, $^3J_{\text{H-H}} = 7.9$, 1H, CH_{arom}), 7.08 (d, $^3J_{\text{H-H}} = 7.6$, 1H, CH_{arom}), 6.92 (d, $^3J_{\text{H-H}} = 7.5$, 1H, CH_{arom}), 4.46 (m, 1H, CH COD), 4.38 (m, 1H, CH COD), 3.55 (m, 1H, CH COD), 3.50 (m, 1H, CH COD), 3.17 (s, 3H, CH_3), 2.36 (m, 3H, CH_2 COD), 2.24 (s, 3H, CH_3), 1.98 (m, 1H, CH_2 COD), 1.70 (m, 2H, CH_2 COD), 1.66 (m, 1H, CH_2 COD), 1.46 (m, 1H, CH_2 COD). ^{13}C -APT NMR (100.6 MHz, CD_2Cl_2 , 213 K): δ 159.5, 159.4, 159.0, 156.0, 153.0, 152.9 (all s, C_{arom}), 139.2, 138.7 (both s, CH_{arom}), 135.8, 133.3 (both s, C_{arom}), 132.6, 132.0, 123.6, 122.2, 121.0, 120.3, 120.2, 113.7 (all s, CH_{arom}), 81.7 (d, $^2J_{\text{C-Rh}} = 12.2$, CH COD), 80.4 (d, $^2J_{\text{C-Rh}} = 11.5$, CH COD), 75.6 (d, $^2J_{\text{C-Rh}} = 13.6$, CH COD), 74.6 (d, $^2J_{\text{C-Rh}} = 13.4$, CH COD), 31.4, 30.3, 30.0, 29.9 (all s, CH_2 COD), 25.5, 24.2 (both s, py-CH_3).

Addition of 1.0 mol of HBMePHI to $[\text{Rh}(\mu\text{-Cl})(\eta^4-C_8H_{12})]_2$. At room temperature, 10 mg (0.03 mmol) of HBMePHI was added to 0.5 mL of a dichloromethane- d_2 solution of 1 (15 mg, 0.03 mmol) in an NMR tube. After 10 min, ^1H NMR spectra between 283 and 183 K (Figure S14) and the $^{13}\text{C}\{^1\text{H}\}$ NMR spectrum at 183 K (Figure S15) were recorded. HRMS (electrospray, m/z): calcd for $\text{C}_{36}\text{H}_{41}\text{Rh}_2\text{N}_5\text{Cl}$ [$M - \text{Cl}$]⁺ 784.1155, found 784.1190. Selected spectroscopic data for $\text{RhCl}(\eta^4-C_8H_{12})\{\mu-N_{py}, N_{py}-(\text{HBMePHI})\}$ (6): are as follows. ^1H NMR (400 MHz, CD_2Cl_2 , 183 K): δ 8.1–8.0 (3H, CH_{arom}), 7.8–7.7 (4H, CH_{arom}), 7.1–7.0 (3H, CH_{arom}), 4.50 (br, 1H, CH COD), 4.44 (br, 1H, CH COD), 3.48 (br, 1H, CH COD), 3.42 (br, 1H, CH COD), 2.80 (s, 6H, py-CH_3), 2.40 (m, 4H, CH_2 COD), 2.33 (m, 4H, CH_2 COD), 1.66 (m, 8H, CH_2 COD). $^{13}\text{C}\{^1\text{H}\}$ -APT NMR (100.6 MHz, CD_2Cl_2 , 193 K): δ 158.6, 158.4, 157.5 (all s, C_{arom}), 139.1 (s, 2C, CH_{arom}), 133.7 (s, C_{arom}), 132.7, 121.1 (s, 2C, CH_{arom}), 81.8, 80.8, 76.1, 75.7 (all br, CH COD), 30.8, 30.2, 29.9, 29.6 (all s, CH_2 COD), 24.9 (s, 2C, py-CH_3).

Preparation of $\text{IrCl}(\eta^4\text{-C}_8\text{H}_{12})\{\kappa^1\text{-N}_{\text{py}}\text{-(HBMePHI)}\}$ (7). Complex 2 (0.300 g, 0.446 mmol) was dissolved in toluene (6 mL) and treated with 2.0 mol of HBMePHI (0.320 g, 0.981 mmol). The resulting suspension turned red and was stirred for 2 h. Then, the volatiles were removed under vacuum. The residue was washed with pentane (3×3 mL) to afford a red solid, which was dried *in vacuo*. Yield: 323 mg (54%). Red crystals suitable for X-ray diffraction analysis were obtained from slow diffusion of pentane in a concentrated solution of 7 in toluene. Anal. Calcd for $\text{C}_{28}\text{H}_{29}\text{ClIrN}_5$: C, 50.71; H, 4.41; N, 10.56. Found: C, 50.37; H, 4.59; N, 10.55. HRMS (electrospray, m/z): calcd for $\text{C}_{28}\text{H}_{29}\text{IrN}_5$ $[\text{M} - \text{Cl}]^+$ 628.2046, found 628.2047. ^1H NMR (400 MHz, CD_2Cl_2 , 243 K): δ 12.72 (s, 1 H, NH), 8.61 (dd, $^3J_{\text{H-H}} = 6.2$, $^3J_{\text{H-H}} = 1.6$, CH_{iso}), 8.03 (dd, $^3J_{\text{H-H}} = 6.2$, $^3J_{\text{H-H}} = 1.6$, 1H, CH_{iso}), 7.81–7.80 (m, 2H, CH_{arom}), 7.76 (dd, $^3J_{\text{H-H}} = 7.6$, $^3J_{\text{H-H}} = 7.6$, 1H, CH_{py}), 7.66 (m, 1H, CH_{py}), 7.22 (d, 1H, $^3J_{\text{H-H}} = 8.3$, CH_{py}), 7.20 (d, 1H, $^3J_{\text{H-H}} = 8.3$, CH_{py}), 7.13 (d, 1H, $^3J_{\text{H-H}} = 7.6$, CH_{py}), 6.94 (d, 1H, $^3J_{\text{H-H}} = 7.6$, CH_{py}), 4.23 (m, 1H, = CH COD), 4.10 (m, 1H, = CH COD), 3.22 (m, 1H, = CH COD), 3.12 (m, 1H, = CH COD), 3.03 (s, 3 H, CH_3), 2.27 (s, 3 H, CH_3), 2.15 (m, 3 H, CH_2 COD), 1.99 (m, 1 H, CH_2 COD), 1.72 (m, 1 H, CH_2 COD), 1.38 (m, 4 H, COD), 1.12 (m, 1 H, COD). $^{13}\text{C}\{^1\text{H}\}$ -APT NMR (plus HSQC and HMBC) (100.6 MHz, CD_2Cl_2 , 243 K): δ 159.6, 159.5, 159.4, 156.3 (all s, C_{py}), 153.2, 152.5 (both s, C_{iso}) 139.2, 139.0 (both s, CH_{py}) 136.1, 133.5 (both s, C_{iso}) 132.7, 132.3, 124.0, 122.5 (all s, CH_{iso}), 121.8, 120.6, 120.4, 114.6 (all s, CH_{py}) 66.3, 64.3, 58.1, 57.4 (all s, =CH COD) 32.2, 31.3 (both s, CH_2 COD) 31.0 (s, 2 C, CH_2 COD), 25.3, 24.4 (both s, py-CH_3).

Preparation of $\{\text{IrCl}(\eta^4\text{-C}_8\text{H}_{12})\}_2(\mu\text{-N}_{\text{py}}\text{N}_{\text{py}}\text{-HBMePHI})$ (8). Complex 2 (0.300 g, 0.446 mmol) was dissolved in toluene (8 mL) and treated with 1.0 mol of HBMePHI (0.145 g, 0.446 mmol). The orange suspension turned red, and a yellow precipitate was formed. After 4 h, at room temperature, the solid was separated from the liquors. The yellow solid was washed with pentane (3×3 mL, 273 K) and was dried *in vacuo*. Yield: 357 mg (80%). Yellow crystals suitable for X-ray diffraction analysis were obtained from slow diffusion of diethyl ether in a concentrated solution of 8 in dichloromethane. Anal. Calcd for $\text{C}_{36}\text{H}_{41}\text{Cl}_2\text{Ir}_2\text{N}_5$: C, 43.28; H, 4.14; N, 7.01. Found: C, 42.88; H, 3.79; N, 7.34. HRMS (electrospray, m/z): calcd for $\text{C}_{36}\text{H}_{41}\text{Ir}_2\text{N}_5\text{Cl}$ $[\text{M} - \text{Cl}]^+$ 964.2304, found 964.2286. ^1H NMR (400 MHz, CD_2Cl_2 , 253 K): δ 12.70 (s, 1H, NH), 8.83 (m, 2H, CH_{arom}), 7.92 (m, 2H, CH_{arom}), 7.62 (m, 2H, CH_{arom}), 7.33 (d, 2H, $^3J_{\text{H-H}} = 8.1$, CH_{arom}), 7.02 (d, 2H, $^3J_{\text{H-H}} = 8.1$, CH_{arom}), 4.25 (m, 2H, CH COD), 4.05 (m, 2H, CH COD), 3.58 (m, 2H, CH COD), 3.25 (m, 2H, CH COD), 2.85 (s, 6H, py-CH_3), 2.19 (m, 2H, CH_2 COD), 1.99 (m, 2H, CH_2 COD), 1.51 (m, 2H, CH_2 COD), 1.41 (m, 2H, CH_2 COD). $^{13}\text{C}\{^1\text{H}\}$ -APT NMR (100.6 MHz, CD_2Cl_2 , 253 K): δ 159.6, 158.2, 152.6 (all s, C_{arom}) 139.4 (s, CH_{arom}), 134.6 (s, C_{arom}), 133.0, 124.6, 121.9, 116.4 (all s, CH_{arom}), 66.1, 65.8, 59.1, 58.6 (all s, =CH COD), 32.4, 31.9, 31.3, 30.8 (all s, CH_2 COD), 25.2 (s, py-CH_3).

Preparation of $\{\text{Rh}(\eta^4\text{-C}_8\text{H}_{12})\}_2(\mu\text{-OH})(\mu\text{-N}_{\text{iso}}\text{N}_{\text{py}}\text{-BMePHI})$ (9). The substrate HBMePHI (0.071 g, 0.219 mmol) was added to 3 mL of a propan-2-ol suspension of 3 (0.1 g, 0.219 mmol). After 2 h an orange solid was formed. The liquors were separated, and the orange solid was washed with 2 mL of propan-2-ol at 0 °C. The solid was solved in toluene. The solution was concentrated *in vacuo*. The addition of pentane gives rises to the precipitation of an orange solid which was washed with pentane (2×3 mL) at 0 °C. Yield: 132 mg (80%). Orange crystals of 9 were obtained from slow diffusion of pentane in toluene. Anal. Calcd for $\text{C}_{36}\text{H}_{41}\text{N}_5\text{ORh}_2$: C, 56.48; H, 5.40; N, 9.15. Found: C, 56.20; H, 5.35; N, 9.28. HRMS (electrospray, m/z): calcd for $\text{C}_{36}\text{H}_{40}\text{N}_5\text{Rh}_2$ $[\text{M} - \text{OH}]^+$ 748.1388, found 748.1392. ^1H NMR (400 MHz, toluene- d_8 , 183 K): δ 8.43 (dd, $^3J_{\text{H-H}} = 4.1$, 3.0, 1H, CH_{arom}), 8.31 (dd, $^3J_{\text{H-H}} = 4.1$, 3.0, 1H, CH_{arom}), 7.30 (d, $^3J_{\text{H-H}} = 7.8$, 1H, CH_{arom}), 7.22 (m, 1H, CH_{arom}), 7.14 (m, 1H, CH_{arom}), 7.07 (m, 1H, CH_{arom}), 6.98 (d, $^3J_{\text{H-H}} = 7.8$, 1H, CH_{arom}), 6.88 (dd, $^3J_{\text{H-H}} = 7.8$, 7.8, 1H, CH_{arom}), 6.41 (d, $^3J_{\text{H-H}} = 7.5$, 1H, CH_{arom}), 6.22 (d, $^3J_{\text{H-H}} = 7.5$, 1H, CH_{arom}), 5.34 (m, 1H, CH COD), 4.31 (m, 1H, CH COD), 4.02 (m, 1H, CH COD), 3.64 (m, 1H, CH COD), 3.48 (m, 1H, CH COD), 3.36 (m, 1H, CH COD), 3.27 (m, 1H, CH COD), 3.21 (m, 1H, CH COD), 3.18 (s,

3H, py-CH_3), 2.44 (m, 2H, CH_2 COD), 2.40 (s, 3H, py-CH_3), 2.22 (s, 1H, Rh–OH–Rh), 1.86 (m, 2H, CH_2 COD), 1.74 (m, 2H, CH_2 COD), 1.56 (m, 2H, CH_2 COD), 1.31 (m, 2H, CH_2 COD), 1.26 (m, 2H, CH_2 COD), 1.12 (m, 2H, CH_2 COD), 1.01 (m, 2H, CH_2 COD). $^{13}\text{C}\{^1\text{H}\}$ -APT NMR (100.6 MHz, toluene- d_8 , 193 K): δ 166.5, 165.1, 164.2, 161.0, 158.6, 156.6, 141.9, 140.9 (all s, C_{arom}), 138.7, 138.4, 131.0, 130.6, 122.3, 121.6, 118.0, 117.9, 117.4, 116.7 (all s, CH_{arom}), 83.7, 81.8, 81.0, 79.3, 74.7, 72.9, 71.5, 71.3 (all s, CH COD), 34.2 (s, CH_2 COD), 31.7 (s, 2C, CH_2 COD), 31.2, 30.1, 29.9, 29.3, 28.9 (all s, CH_2 COD), 26.5 (py-CH_3), 25.3 (py-CH_3).

Preparation of $\{\text{Ir}(\eta^4\text{-C}_8\text{H}_{12})\}_2(\mu\text{-OH})(\mu\text{-N}_{\text{iso}}\text{N}_{\text{py}}\text{-BMePHI})$ (10). The substrate HBMePHI (0.051 g, 0.157 mmol) was added to 3 mL of a propan-2-ol suspension of 4 (0.1 g, 0.157 mmol). After 2 h an orange solid was formed. The liquors were separated, and the orange solid was washed with 2 mL of propan-2-ol at 0 °C. The solid was solved in toluene. The solution was concentrated *in vacuo*. The addition of pentane gives rise to the precipitation of an orange solid, which was washed with pentane (2×3 mL) at 0 °C. Yield: 70 mg (47%). Orange crystals of 10 were obtained from slow diffusion of pentane in toluene. Anal. Calcd for $\text{C}_{36}\text{H}_{41}\text{Ir}_2\text{N}_5\text{O}$: C, 45.80; H, 4.38; N, 7.42. Found: C, 46.10; H, 4.26; N, 7.52. HRMS (electrospray, m/z): calcd for $\text{C}_{36}\text{H}_{40}\text{Ir}_2\text{N}_5$ $[\text{M} - \text{OH}]^+$ 928.2537, found 928.2585. ^1H NMR (400 MHz, toluene- d_8 , 193 K): δ 8.28 (br, 1H, CH_{arom}), 8.20 (br, 1H, CH_{arom}), 7.13 (br, 3H, CH_{arom}), 7.08 (br, 1H, CH_{arom}), 6.90 (br, 1H, CH_{arom}), 6.77 (br, 1H, CH_{arom}), 6.32 (br, 1H, CH_{arom}), 6.09 (br, 1H, CH_{arom}), 5.07 (br, 1H, CH COD), 4.24 (br, 1H, Ir–OH–Ir), 4.05 (br, 1H, CH COD), 3.86 (br, 1H, CH COD), 3.44 (br, 1H, CH COD), 3.20 (br, 3H, CH COD), 2.99 (br, 1H, CH COD), 2.87 (s, 3H, py-CH_3), 2.33 (s, 3H, py-CH_3), 2.32 (br, 2H, CH_2 COD), 1.86 (br, 2H, CH_2 COD), 1.68 (br, 2H, CH_2 COD), 1.44 (br, 2H, CH_2 COD), 1.36 (br, 2H, CH_2 COD), 1.09 (br, 2H, CH_2 COD), 0.98 (br, 2H, CH_2 COD), 0.82 (br, 2H, CH_2 COD). $^{13}\text{C}\{^1\text{H}\}$ -APT NMR (plus HSQC and HMBC) (100.6 MHz, toluene- d_8 , 188 K): δ 165.4, 164.9, 163.8, 159.2, 157.0, 155.7, 140.8, 139.9 (all s, C_{arom}), 138.1, 138.0, 130.7, 130.3, 122.0, 121.4, 118.2, 118.0, 116.9, 116.3 (all s, CH_{arom}), 67.4, 66.5, 65.6, 62.4, 56.3, 55.2, 53.0, 52.2 (all s, CH COD), 34.6, 32.3, 32.2, 31.7, 30.7, 30.2, 30.1, 29.0 (all s, CH_2 COD), 25.6, 24.7 (both s, py-CH_3).

Preparation of $\{\text{Rh}(\eta^4\text{-C}_8\text{H}_{12})\}_2(\mu\text{-N}_{\text{iso}}\text{N}_{\text{imine}}\text{-(HN=C}_8\text{H}_4\text{NO)})\text{-}(\mu\text{-N=C}_8\text{H}_4\text{NO}^{\text{Pr}})$ (11). The substrate HBMePHI (173.2 mg, 0.531 mmol) and KO^tBu (89 mg, 0.796 mmol) were added to 3 mL of a propan-2-ol suspension of 3 (121 mg, 0.265 mmol). The mixture was stirred for 2 h at room temperature, and an orange solid was formed, which was filtered off. The filtrate was cooled at 4 °C for 3 days, and red crystals were obtained. Yield: 40 mg (20%). Anal. Calcd for $\text{C}_{35}\text{H}_{40}\text{N}_4\text{O}_2\text{Rh}_2$: C, 55.71; H, 5.34; N, 7.43. Found: C, 55.87; H, 5.42; N, 7.38. HRMS (electrospray, m/z): calcd for $\text{C}_{35}\text{H}_{41}\text{N}_4\text{O}_2\text{Rh}_2$ $[\text{M} + \text{H}]^+$ 755.1334, found 755.1308. ^1H NMR (400 MHz, C_6D_6 , 298 K): δ 10.61 (d, $^3J_{\text{H-H}} = 7.5$, 1 H, CH_{arom}), 7.65 (t, $^3J_{\text{H-H}} = 7.5$, 1 H, CH_{arom}), 7.39 (d, $^3J_{\text{H-H}} = 7.3$, 1 H, CH_{arom}), 7.27 (d, $^3J_{\text{H-H}} = 7.3$, 1 H, CH_{arom}), 7.02 (dd, $^3J_{\text{H-H}} = 7.4$, 7.2, 1 H, CH_{arom}), 6.74 (dd, $^3J_{\text{H-H}} = 7.4$, 7.2, 1 H, CH_{arom}), 6.64 (dd, $^3J_{\text{H-H}} = 7.4$, 7.2, 1 H, CH_{arom}), 6.44 (m, 1 H, CH COD), 6.25 (d, $^3J_{\text{H-H}} = 7.5$, 1 H, CH_{arom}), 6.21 (m, 1 H, CH COD), 5.78 (br, 1 H, NH), 5.36 (sept, $^3J_{\text{H-H}} = 6.4$, 1H, $\text{OCH}(\text{CH}_3)_2$), 5.15 (m, 1 H, CH COD), 4.98 (dd, $^3J_{\text{H-H}} = 7.2$, 6.9, 1 H, CH COD), 4.54 (dd, $^3J_{\text{H-H}} = 7.2$, 6.9, 1 H, CH COD), 3.96 (dd, $^3J_{\text{H-H}} = 7.2$, 6.9, 1 H, CH COD), 3.55 (m, 1 H, CH COD), 3.44 (m, 1 H, CH COD), 3.23 (m, 2 H, CH_2 COD), 3.11 (m, 2 H, CH_2 COD), 2.36 (m, 6 H, CH_2 COD), 2.16 (m, 2 H, CH_2 COD), 1.67 (m, 4 H, CH_2 COD), 1.26 and 1.15 (both d, $^3J_{\text{H-H}} = 6.4$, 3 H each, $\text{OCH}(\text{CH}_3)_2$). $^{13}\text{C}\{^1\text{H}\}$ -APT NMR (plus HSQC and HMBC) (100.6 MHz, CD_2Cl_2 , 298 K): δ 176.8, 175.3, 174.5, 163.8, 136.5, 136.0, 134.9, 134.6 (all s, C_{arom}), 130.8, 130.6, 129.8, 128.8, 125.9, 121.9, 119.1, 118.4 (all s, CH_{arom}), 86.9 (d, $^2J_{\text{C-Rh}} = 12.9$, CH COD), 84.2 (d, $^2J_{\text{C-Rh}} = 8.9$, CH COD), 81.9 (d, $^2J_{\text{C-Rh}} = 11.7$, CH COD), 81.6 (d, $^2J_{\text{C-Rh}} = 10.5$, CH COD) 81.2 (d, $^2J_{\text{C-Rh}} = 10.5$, CH COD), 79.0 (d, $^2J_{\text{C-Rh}} = 10.5$, CH COD), 78.2 (d, $^2J_{\text{C-Rh}} = 12.9$, CH COD), 74.5 (d, $^2J_{\text{C-Rh}} = 11.7$, CH COD), 72.2 (s, $\text{OCH}(\text{CH}_3)_2$), 35.2, 35.2, 35.0, 34.3, 29.5, 29.0, 28.6, 28.5 (all s, CH_2 COD), 22.0 and 21.9 (both s, OCHCH_3).

Preparation of $\text{Ir}_3(\eta^4\text{-C}_8\text{H}_{12})_2(\kappa^1\text{-C}_8\text{H}_{13})(\mu\text{-OH})(\text{L})$ (12). The substrate HBMepHI (147 mg, 0.450 mmol) and KO^tBu (75 mg, 0.675 mmol) were added to 4 mL of a propan-2-ol suspension of **4** (142 mg, 0.225 mmol). The mixture was stirred for 2 h at room temperature, and an orange solid was formed, which was filtered off and subsequently was treated with toluene (2×4 mL) to afford a yellow solid and a red solution. The solution was separated by filtration, and the volatiles were removed under vacuum. The treatment of the residue with pentane gave an orange solid. Orange crystals suitable for X-ray diffraction analysis were obtained from a saturated solution in benzene. Yield: 42 mg (22%). Anal. Calcd for $\text{C}_{44}\text{H}_{54}\text{Ir}_3\text{N}_5\text{O}$: C, 42.43; H, 4.37; N, 5.62. Found: C, 42.18; H, 4.38; N, 5.39. HRMS (electrospray, m/z): calculated for $\text{C}_{44}\text{H}_{53}\text{Ir}_3\text{N}_5$ [$\text{M} - \text{OH}$] $^+$ 1230.3183, found 1230.3152. ^1H NMR (500.13 MHz, C_6D_6 , 298 K): δ 8.53 (dd, $^3J_{\text{H-H}} = 7.8$, 1.0, 1H, H^{12}), 8.07 (dd, $^3J_{\text{H-H}} = 7.3$, 1.4, 1H, H^9), 7.64 (dd, $^3J_{\text{H-H}} = 7.9$, 1.0, 1H, CH_{py}), 7.29 (m, 2H, CH_{arom}), 7.25 (dd, $^3J_{\text{H-H}} = 7.4$, 1.4, 1H, H^{11}), 7.14 (m, 1H, CH_{py}), 7.13 (m, 1H, CH_{py}), 6.69 (dd, $^3J_{\text{H-H}} = 7.3$, 1.0, 1H, CH_{py}), 5.94 (d, $^3J_{\text{H-H}} = 7.2$, 1H, CH_{py}), 5.55 (m, 1H, CH COD), 4.54 (m, 1H, CH COD), 4.12 (m, 1H, CH COD), 4.04 (m, 1H, CH COD), 3.88 (m, 1H, CH COD), 3.82 (m, 1H, CH COD), 3.69 (m, 1H, CH COD), 3.46 (m, 1H, CH COD), 3.37 (s, 3H, py-CH_3), 3.11 (m, 2H, CH COD), 2.58 (m, 1H, CH_2 COD), 2.50 (m, 1H, CH_2 COD), 2.32 (m, 1H, CH_2 COD), 2.29 (m, 1H, CH_2 COD), 2.13 (m, 3H, CH_2 COD), 2.04 (m, 3H, CH_2 COD), 1.94 (m, 4H, CH_2 COD), 1.85 (s, 3H, py-CH_3), 1.79 (m, 1H, CH_2 COD), 1.75 (m, 1H, CH_2 COD), 1.20 (m, 3H, CH_2 COD), 1.11 (m, 2H, CH_2 COD), 0.65 (m, 1H, $\kappa^1\text{-CH COD}$), 0.24 (s, 1H, Ir-OH-Ir). $^{13}\text{C}\{^1\text{H}\}$ -APT NMR (plus HSQC and HMBC) (75 MHz, C_6D_6 , 298 K): δ 198.9 (s, C^7), 179.3 (s, C_{py}), 166.7 (s, C_{py}), 159.4 (s, C^{14}), 157.9 (s, C_{py}), 153.1 (s, C_{py}), 145.8 (s, C^{13}), 137.7 (s, C_{py}), 137.6 (s, C_{py}), 135.4 (s, C^8), 129.1 (s, C^{12}), 128.8 (s, C^{11}), 127.9 (s, C^{10}), 122.3 (s, C^9), 119.6 (s, C_{py}), 117.6 (s, C_{py}), 111.1 (s, C_{py}), 110.3 (s, C_{py}), 86.4, 71.4, 67.7, 67.0, 63.0, 60.1, 59.7, 59.0, 59.0, 52.6 (all s, = CH COD), 42.7, 36.9, 35.8, 34.5, 32.6, 32.5 (all s, CH_2 COD), 32.1 ($\kappa^1\text{-CH COD}$), 31.1, 30.7, 30.3, 29.5, 28.5, 28.2 (all s, CH_2 COD), 25.0 (s, py-CH_3), 23.4 (s, CH_2 COD), 21.0 (s, py-CH_3).

■ ASSOCIATED CONTENT

■ Supporting Information

The Supporting Information is available free of charge at <https://pubs.acs.org/doi/10.1021/acs.organomet.1c00068>.

Computational and electrochemical data, structural analysis of complexes **7–9**, **11**, and **12**, and NMR spectra (PDF)

Cartesian coordinates of computed complexes (XYZ)

Accession Codes

CCDC 1913552–1913556 contain the supplementary crystallographic data for this paper. These data can be obtained free of charge via www.ccdc.cam.ac.uk/data_request/cif, or by emailing data_request@ccdc.cam.ac.uk, or by contacting The Cambridge Crystallographic Data Centre, 12 Union Road, Cambridge CB2 1EZ, UK; fax: +44 1223 336033.

■ AUTHOR INFORMATION

Corresponding Authors

Miguel A. Esteruelas – Departamento de Química Inorgánica, Instituto de Síntesis Química y Catálisis Homogénea (ISQCH), Centro de Innovación en Química Avanzada (ORFEO-CINQA), Universidad de Zaragoza-CSIC, 50009 Zaragoza, Spain; orcid.org/0000-0002-4829-7590; Email: maester@unizar.es

Miguel A. Sierra – Departamento de Química Orgánica I, Facultad de CC. Químicas, Centro de Innovación en Química Avanzada (ORFEO-CINQA), Universidad Complutense de

Madrid, 28040 Madrid, Spain; orcid.org/0000-0002-3360-7795; Email: sierraor@ucm.es

Authors

María L. Buil – Departamento de Química Inorgánica, Instituto de Síntesis Química y Catálisis Homogénea (ISQCH), Centro de Innovación en Química Avanzada (ORFEO-CINQA), Universidad de Zaragoza-CSIC, 50009 Zaragoza, Spain; orcid.org/0000-0002-3284-1053

Alba Collado – Departamento de Química Orgánica I, Facultad de CC. Químicas, Centro de Innovación en Química Avanzada (ORFEO-CINQA), Universidad Complutense de Madrid, 28040 Madrid, Spain; orcid.org/0000-0001-6215-1822

Mar Gómez-Gallego – Departamento de Química Orgánica I, Facultad de CC. Químicas, Centro de Innovación en Química Avanzada (ORFEO-CINQA), Universidad Complutense de Madrid, 28040 Madrid, Spain; orcid.org/0000-0002-8961-7685

Susana Izquierdo – Departamento de Química Inorgánica, Instituto de Síntesis Química y Catálisis Homogénea (ISQCH), Centro de Innovación en Química Avanzada (ORFEO-CINQA), Universidad de Zaragoza-CSIC, 50009 Zaragoza, Spain

Antonio I. Nicasio – Departamento de Química Inorgánica, Instituto de Síntesis Química y Catálisis Homogénea (ISQCH), Centro de Innovación en Química Avanzada (ORFEO-CINQA), Universidad de Zaragoza-CSIC, 50009 Zaragoza, Spain; orcid.org/0000-0002-2268-4920

Enrique Oñate – Departamento de Química Inorgánica, Instituto de Síntesis Química y Catálisis Homogénea (ISQCH), Centro de Innovación en Química Avanzada (ORFEO-CINQA), Universidad de Zaragoza-CSIC, 50009 Zaragoza, Spain; orcid.org/0000-0003-2094-719X

Complete contact information is available at:

<https://pubs.acs.org/doi/10.1021/acs.organomet.1c00068>

Notes

The authors declare no competing financial interest.

■ ACKNOWLEDGMENTS

Financial support from the MCI, projects CTQ2017-82935-P, PID2019-108429RB-I00, and RED2018-102387-T, the Gobierno de Aragón (Group E06_17R), Fundación Ramón Areces (XVIII Concurso Nacional de Ayudas a la Investigación en Ciencias de la Vida y de la Materia CIVP18A3938), Fondo Europeo de Desarrollo Regional (FEDER), and the European Social Fund (FSE) is acknowledged. A.I.N. and A.C. thank the MINECO (Spain) for a predoctoral fellowship and Juan de la Cierva-Incorporación Fellowship, respectively.

■ REFERENCES

- (a) Tojo, G.; Fernández, M. *Oxidations of Alcohols to Aldehydes and Ketones*; Springer: Heidelberg, Germany, 2006; pp 1–148. (b) Arend, W. C. E.; Sheldon, R. A. *Modern Oxidation Methods*; Backvall, J.-E., Ed.; Wiley-VCH: Weinheim, Germany, 2010; Vol. 2, pp 147–180.
- (a) Shi, Z.; Zhang, C.; Tang, C.; Jiao, N. Recent advances in transition-metal catalyzed reactions using molecular oxygen as the oxidant. *Chem. Soc. Rev.* **2012**, *41*, 3381–3430. (b) Kopylovich, M. N.; Ribeiro, A. P. C.; Alegria, E. C. B. A.; Martins, N. M. R.; Martins, L. M. D. R. S.; Pombeiro, A. J. L.; Pérez, P. J. Catalytic Oxidation of Alcohols: Recent Advances. *Adv. Organomet. Chem.* **2015**, *63*, 91–174.

- (3) (a) Friedrich, A.; Schneider, S. Acceptorless Dehydrogenation of Alcohols: Perspectives for Synthesis and H₂ Storage. *ChemCatChem* **2009**, *1*, 72–73. (b) Trincado, M.; Banerjee, D.; Grützmacher, H. Molecular Catalysts for Hydrogen Production from Alcohols. *Energy Environ. Sci.* **2014**, *7*, 2464–2503. (c) Werkmeister, S.; Neumann, J.; Junge, K.; Beller, M. Pincer-Type Complexes for Catalytic (De)-Hydrogenation and Transfer (De)Hydrogenation Reactions: Recent Progress. *Chem. - Eur. J.* **2015**, *21*, 12226–12250. (d) Nielsen, M. In *Hydrogen Pollution and Remediation Carbon and Pollutants*; Lichtfouse, E., Schwarzbauer, J., Robert, D., Eds.; Springer International: Cham, Switzerland, 2015; pp 2–6. (e) Crabtree, R. H. Homogeneous Transition Metal Catalysis of Acceptorless Dehydrogenative Alcohol Oxidation: Applications in Hydrogen Storage and to Heterocycle Synthesis. *Chem. Rev.* **2017**, *117*, 9228–9246.
- (4) (a) Jing, Y.; Chen, X.; Yang, X. Computational Mechanistic Study of the Hydrogenation and Dehydrogenation Reactions Catalyzed by Cobalt Pincer Complexes. *Organometallics* **2015**, *34*, 5716–5722. (b) Hou, C.; Zhang, Z.; Zhao, C.; Ke, Z. DFT Study of Acceptorless Alcohol Dehydrogenation Mediated by Ruthenium Pincer Complexes: Ligand Tautomerization Governing Metal Ligand Cooperation. *Inorg. Chem.* **2016**, *55*, 6539–6551.
- (5) (a) Zhang, J.; Gandelman, M.; Shimon, L. J. W.; Rozenberg, H.; Milstein, D. Electron-Rich, Bulky Ruthenium PNP-Type Complexes. Acceptorless Catalytic Alcohol Dehydrogenation. *Organometallics* **2004**, *23*, 4026–4033. (b) Zhang, J.; Leitun, G.; Ben-David, Y.; Milstein, D. Facile Conversion of Alcohols into Esters and Dihydrogen Catalyzed by New Ruthenium Complexes. *J. Am. Chem. Soc.* **2005**, *127*, 10840–10841. (c) Musa, S.; Shaposhnikov, I.; Cohen, S.; Gelman, D. Ligand-Metal Cooperation in PCP Pincer Complexes: Rational Design and Catalytic Activity in Acceptorless Dehydrogenation of Alcohols. *Angew. Chem., Int. Ed.* **2011**, *50*, 3533–3537. (d) Kamitani, M.; Ito, M.; Itazaki, M.; Nakazawa, H. Effective Dehydrogenation of 2-Pyridylmethanol Derivatives Catalyzed by an Iron Complex. *Chem. Commun.* **2014**, *50*, 7941–7944. (e) Song, H.; Kang, B.; Hong, S. H. Fe-Catalyzed Acceptorless Dehydrogenation of Secondary Benzylic Alcohols. *ACS Catal.* **2014**, *4*, 2889–2895. (f) Sengupta, D.; Bhattacharjee, R.; Pramanick, R.; Rath, S. P.; Saha Chowdhury, N.; Datta, A.; Goswami, S. Exclusively Ligand-Mediated Catalytic Dehydrogenation of Alcohols. *Inorg. Chem.* **2016**, *55*, 9602–9610. (g) Dutta, I.; Sarbajna, A.; Pandey, P.; Rahaman, S. M. W.; Singh, K.; Bera, J. K. Acceptorless Dehydrogenation of Alcohols on a Diruthenium(II,II) Platform. *Organometallics* **2016**, *35*, 1505–1513. (h) Toyomura, K.; Fujita, K. Synthesis of Coordinatively Unsaturated Iridium Complexes Having Functional 8-Quinolinolato Ligands: New Catalysts for Dehydrogenative Oxidation of Alcohols in Aqueous Media. *Chem. Lett.* **2017**, *46*, 808–810. (i) Wang, Z.; Pan, B.; Liu, Q. B.; Yue, E. L.; Solan, G. A.; Ma, Y. P.; Sun, W.-H. Efficient Acceptorless Dehydrogenation of Secondary Alcohols to Ketones Mediated by a PNN-Ru(II) Catalyst. *Catal. Sci. Technol.* **2017**, *7*, 1654–1661. (j) Wang, Q.; Chai, H.; Yu, Z. Dimeric Ruthenium(II)-NNN Complex Catalysts Bearing a Pyrazolyl-Pyridylamino-Pyridine Ligand for Transfer Hydrogenation of Ketones and Acceptorless Dehydrogenation of Alcohols. *Organometallics* **2017**, *36*, 3638–3644. (k) Huang, R.; Yang, Y.; Wang, D.-S.; Zhang, L.; Wang, D. Where does Au Coordinate to N-(2-pyridyl)Benzotriazole: Gold-Catalyzed Chemoselective Dehydrogenation and Borrowing Hydrogen Reactions. *Org. Chem. Front.* **2018**, *5*, 203–209. (l) Hao, Z.; Liu, K.; Feng, Q.; Dong, Q.; Ma, D.; Han, Z.; Lu, G.-L.; Lin, J. Ruthenium(II) Complexes Bearing Schiff Base Ligands for Efficient Acceptorless Dehydrogenation of Secondary Alcohols. *Chin. J. Chem.* **2021**, *39*, 121–128.
- (6) (a) van Buijtenen, J.; Meuldijk, J.; Vekemans, J. A. J. M.; Hulshof, L. A.; Kooijman, H.; Spek, A. L. Dinuclear Ruthenium Complexes Bearing Dicarboxylate and Phosphine Ligands. Acceptorless Catalytic Dehydrogenation of 1-Phenylethanol. *Organometallics* **2006**, *25*, 873–881. (b) Zhang, J.; Balaraman, E.; Leitun, G.; Milstein, D. Electron-Rich PNP- and PNN-Type Ruthenium(II) Hydrido Borohydride Pincer Complexes. Synthesis, Structure, and Catalytic Dehydrogenation of Alcohols and Hydrogenation of Esters. *Organometallics* **2011**, *30*, 5716–5724. (c) Kawahara, R.; Fujita, K.-I.; Yamaguchi, R. Cooperative Catalysis by Iridium Complexes with a Bipyridonate Ligand: Versatile Dehydrogenative Oxidation of Alcohols and Reversible Dehydrogenation-Hydrogenation between 2-Propanol and Acetone. *Angew. Chem., Int. Ed.* **2012**, *51*, 12790–12794. (d) Muthaiah, S.; Hong, S. H. Acceptorless and Base-Free Dehydrogenation of Alcohols and Amines using Ruthenium-Hydride Complexes. *Adv. Synth. Catal.* **2012**, *354*, 3045–3053. (e) Tseng, K.-N. T.; Kampf, J. W.; Szymczak, N. K. Base-Free, Acceptorless, and Chemoselective Alcohol Dehydrogenation Catalyzed by an Amide-Derived NNN-Ruthenium(II) Hydride Complex. *Organometallics* **2013**, *32*, 2046–2049. (f) Yamaguchi, R.; Kobayashi, D.; Shimizu, M.; Fujita, K.-I. Synthesis of a series of iridium complexes bearing substituted 2-pyridonates and their catalytic performance for acceptorless dehydrogenation of alcohols under neutral conditions. *J. Organomet. Chem.* **2017**, *843*, 14–19. (g) Xu, S.; Althlthol, L. M.; Paudel, K.; Reinheimer, E.; Tyer, D. L.; Taylor, D. K.; Smith, A. M.; Holzmann, J.; Lozano, E.; Ding, K. Tripodal N,P Mixed-Donor Ligands and Their Cobalt Complexes: Efficient Catalysts for Acceptorless Dehydrogenation of Secondary Alcohols. *Inorg. Chem.* **2018**, *57*, 2394–2397. (h) Fanara, P. M.; MacMillan, S. N.; Lacy, D. C. Planar-Locked Ru-PNN Catalysts in 1-Phenylethanol Dehydrogenation. *Organometallics* **2020**, *39*, 3628–3644. (i) Jayaprakash, H.; Guo, L.; Wang, S.; Bruneau, C.; Fischmeister, C. Acceptorless and Base-Free Dehydrogenation of Alcohols Mediated by a Dipyridylamine-Iridium(III) Catalyst. *Eur. J. Org. Chem.* **2020**, *2020*, 4326–4330.
- (7) (a) González Miera, G.; Martínez-Castro, E.; Martín-Matute, B. Acceptorless Alcohol Dehydrogenation: OH vs NH Effect in Bifunctional NHC-Ir(III) Complexes. *Organometallics* **2018**, *37*, 636–644. (b) Wang, Q.; Guo, C.-H.; Zhang, X.; Zhu, M.; Jiao, H.; Wu, H.-S. Mechanisms and Activity of 1-Phenylethanol Dehydrogenation Catalyzed by Bifunctional NHC-Ir^{III} Complex. *Eur. J. Org. Chem.* **2019**, *2019*, 3929–3936.
- (8) (a) Ngo, A. H.; Adams, M. J.; Do, L. H. Selective Acceptorless Dehydrogenation and Hydrogenation by Iridium Catalysts Enabling Facile Interconversion of Glucocorticoids. *Organometallics* **2014**, *33*, 6742–6745. (b) Chakraborty, S.; Lagaditis, P. O.; Förster, M.; Bielinski, E. A.; Hazari, N.; Holthausen, M. C.; Jones, W. D.; Schneider, S. Well-Defined Iron Catalysts for the Acceptorless Reversible Dehydrogenation-Hydrogenation of Alcohols and Ketones. *ACS Catal.* **2014**, *4*, 3994–4003. (c) Fujita, K.-I.; Tamura, R.; Tanaka, Y.; Yoshida, M.; Onoda, M.; Yamaguchi, R. Dehydrogenative Oxidation of Alcohols in Aqueous Media Catalyzed by a Water-Soluble Dicationic Iridium Complex Bearing a Functional N-Heterocyclic Carbene Ligand without Using Base. *ACS Catal.* **2017**, *7*, 7226–7230.
- (9) (a) Esteruelas, M. A.; Oliván, M.; Vélez, A. POP-Pincer Silyl Complexes of Group 9: Rhodium versus Iridium. *Inorg. Chem.* **2013**, *52*, 12108–12119. (b) Esteruelas, M. A.; Fernández, I.; López, A. M.; Mora, M.; Oñate, E. Osmium-Promoted Dehydrogenation of Amine-Boranes and B–H Bond Activation of the Resulting Amine-Boranes. *Organometallics* **2014**, *33*, 1104–1107. (c) Esteruelas, M. A.; López, A. M.; Mora, M.; Oñate, E. Ammonia-Borane Dehydrogenation Promoted by an Osmium Dihydride Complex: Kinetics and Mechanism. *ACS Catal.* **2015**, *5*, 187–191. (d) Bolaño, T.; Esteruelas, M. A.; Gay, M. P.; Oñate, E.; Pastor, I. M.; Yus, M. An Acyl-NHC Osmium Cooperative System: Coordination of Small Molecules and Heterolytic B–H and O–H Bond Activation. *Organometallics* **2015**, *34*, 3902–3908. (e) Esteruelas, M. A.; Nolis, P.; Oliván, M.; Oñate, E.; Vallribera, A.; Vélez, A. Ammonia Borane Dehydrogenation Promoted by a Pincer-Square-Planar Rhodium(I) Monohydride: A Stepwise Hydrogen Transfer from the Substrate to the Catalyst. *Inorg. Chem.* **2016**, *55*, 7176–7181. (f) Esteruelas, M. A.; Lezáun, V.; Martínez, A.; Oliván, M.; Oñate, E. Osmium Hydride Acetylacetonate Complexes and Their Application in Acceptorless Dehydrogenative Coupling of Alcohols and Amines and for the Dehydrogenation of Cyclic Amines. *Organometallics* **2017**, *36*, 2996–3004. (g) Esteruelas, M. A.; García-Yebra, C.; Martín, J.; Oñate, E.

Dehydrogenation of Formic Acid Promoted by a Trihydride-Hydroxo-Osmium(IV) Complex: Kinetics and Mechanism. *ACS Catal.* **2018**, *8*, 11314–11323. (h) Alabau, R. G.; Esteruelas, M. A.; Martínez, A.; Oliván, M.; Oñate, E. Base-Free and Acceptorless Dehydrogenation of Alcohols Catalyzed by an Iridium Complex Stabilized by a *N,N,N*-Osmaligand. *Organometallics* **2018**, *37*, 2732–2740.

(10) (a) Buil, M. L.; Esteruelas, M. A.; Gay, M. P.; Gómez-Gallego, M.; Nicasio, A. I.; Oñate, E.; Santiago, A.; Sierra, M. A. Osmium Catalysts for Acceptorless and Base-Free Dehydrogenation of Alcohols and Amines: Unusual Coordination Modes of a BPI Anion. *Organometallics* **2018**, *37*, 603–617. (b) Buil, M. L.; Esteruelas, M. A.; Izquierdo, S.; Nicasio, A. I.; Oñate, E. N-H and C-H Bond Activations of an Isoindoline Promoted by Iridium- and Osmium-Polyhydride Complexes: A Noninnocent Bridge Ligand for Acceptorless and Base-Free Dehydrogenation of Secondary Alcohols. *Organometallics* **2020**, *39*, 2719–2731. (c) Nicasio, A. I. Ph.D. Dissertation, *Preparación de Catalizadores de Osmio e Iridio para la Deshidrogenación de Líquidos Orgánicos Transportadores de Hidrógeno*; Universidad de Zaragoza, 2021.

(11) (a) Camerano, J. A.; Samann, C.; Wadepohl, H.; Gade, L. H. Bis(pyridylimino)isoindolato-Iridium Complexes as Epoxidation Catalysts for Alkenes. *Organometallics* **2011**, *30*, 379–382. (b) Müller, A. L.; Bleith, T.; Roth, T.; Wadepohl, H.; Gade, L. H. Iridium Half-Sandwich Complexes with Di- and Tridentate Bis(pyridylimino)-isoindolato Ligands: Stoichiometric and Catalytic Reactivity. *Organometallics* **2015**, *34*, 2326–2342.

(12) (a) Kruck, M.; Wadepohl, H.; Enders, M.; Gade, L. H. Giant Residual Dipolar ^{13}C - ^1H Couplings in High-Spin Organoiron Complexes: Elucidation of Their Structures in Solution by ^{13}C NMR Spectroscopy. *Chem. - Eur. J.* **2013**, *19*, 1599–1606. (b) Tran, B. L.; Driess, M.; Hartwig, J. F. Copper-Catalyzed Oxidative Dehydrogenative Carboxylation of Unactivated Alkanes to Allylic Esters via Alkenes. *J. Am. Chem. Soc.* **2014**, *136*, 17292–17301. (c) Roth, T.; Wadepohl, H.; Gade, L. H. Cationic BPI-Gold(III) Complexes: Controlling Ligating and Nonligating Anions. *Eur. J. Inorg. Chem.* **2016**, *2016*, 1184–1191. (d) Gogoi, K.; Saha, S.; Mondal, B.; Deka, H.; Ghosh, S.; Mondal, B. Dioxygenation Reaction of a Cobalt-Nitrosyl: Putative Formation of a Cobalt-Peroxyxynitrite via a $\{\text{Co}^{\text{III}}(\text{NO})(\text{O}_2^-)\}$ Intermediate. *Inorg. Chem.* **2017**, *56*, 14438–14445.

(13) Peris, E.; Lahuerta, P. In *Comprehensive Organometallic Chemistry III: From Fundamentals to Applications*; Mingos, M. P., Crabtree, R. H., Eds.; Elsevier: Amsterdam, 2007; Vol. 7, pp 121–236.

(14) Peruzzini, M.; Bianchini, C.; Gonsalvi, L. In *Comprehensive Organometallic Chemistry III: From Fundamentals to Applications*; Mingos, M. P., Crabtree, R. H., Eds.; Elsevier: Amsterdam, 2007; Vol. 7, pp 265–425.

(15) (a) Calhorda, M. J.; Ceamanos, C.; Crespo, O.; Gimeno, M. C.; Laguna, A.; Larraz, C.; Vaz, P. D.; Villacampa, M. D. Heteropolynuclear Gold Complexes with Metallophilic Interactions: Modulation of the Luminescent Properties. *Inorg. Chem.* **2010**, *49*, 8255–8269. (b) Hale, L. V. A.; McGarry, K. A.; Ringgold, M. A.; Clark, T. B. Role of Hemilabile Diamine Ligands in the Amine-Directed C–H Borylation of Arenes. *Organometallics* **2015**, *34*, 51–55. (c) Murai, M.; Nishinaka, N.; Takai, K. Iridium-Catalyzed Sequential Silylation and Borylation of Heteroarenes Based on Regioselective C,H Bond Activation. *Angew. Chem., Int. Ed.* **2018**, *57*, 5843–5847.

(16) Churchill, M. R.; Bezman, S. A. X-Ray Crystallographic Studies on Fluxional Pentacoordinate Transition-Metal Complexes. III. (Cycloocta-1,5-Diene) [1,3-Bis(Diphenylphosphino)Propane]-Methyliridium(I). *Inorg. Chem.* **1973**, *12*, 531–536.

(17) Pakes, P. W.; Rounds, T. C.; Strauss, H. L. Conformations of Cyclooctane and Some Related Oxocanes. *J. Phys. Chem.* **1981**, *85*, 2469–2475.

(18) Baird, D. M.; Shih, K. Y.; Welch, J. H.; Bereman, R. D. Structural Characterization of Bis(Arylimino)Isoindoline Complexes of Dimolybdenum. *Polyhedron* **1989**, *8*, 2359–2365.

(19) (a) Bröring, M.; Kleeberg, C. Cyclometalation vs. Werner-Type Coordination of Sterically Enforced Palladium(II)-1,3-bis(pyridyl-2-imino)isoindolines (Pd-BPIs). *Dalton Trans.* **2007**, 1101–1103. (b) Bröring, M.; Kleeberg, C.; Tejero, E. C. Syntheses, Structures and Coordination Modes of Acetatepalladium(II) Complexes with 1,3-Bis(2-arylimino)isoindoline Ligands of Different Steric Influence. *Eur. J. Inorg. Chem.* **2007**, *2007*, 3208–3216. (c) Bröring, M.; Kleeberg, C.; Kohler, S. Palladium(II) Complexes of Unsymmetrical CNN pincer ligands. *Inorg. Chem.* **2008**, *47*, 6404–6412.

(20) Zhang, P.; Liao, H.; Wang, H.; Li, X.; Yang, F.; Zhang, S. Cis-1,4-Polymerization of Isoprene Catalyzed by 1,3-Bis(2-pyridylimino)-isoindoline-Ligated Rare-Earth-Metal Dialkyl Complexes. *Organometallics* **2017**, *36*, 2446–2451.

(21) Buil, M. L.; Esteruelas, M. A.; Herrero, J.; Izquierdo, S.; Pastor, I. M.; Yus, M. Osmium Catalyst for the Borrowing Hydrogen Methodology: α -Alkylation of Arylacetonitriles and Methyl Ketones. *ACS Catal.* **2013**, *3*, 2072–2075.

(22) (a) Simon, C.; Constantieux, T.; Rodríguez, J. Utilisation of 1,3-Dicarbonyl Derivatives in Multicomponent Reactions. *Eur. J. Org. Chem.* **2004**, *2004*, 4957–4980. (b) Sabitha, G.; Fatima, N.; Reddy, E. V.; Yadav, J. S. First Examples of Proline-Catalyzed Domino Knoevenagel/Hetero-Diels-Alder/Elimination Reactions. *Adv. Synth. Catal.* **2005**, *347*, 1353–1355.

(23) Dietrich, B. L.; Egbert, J.; Morris, A. M.; Wicholas, M.; Anderson, O. P.; Miller, S. M. Cd(II), Zn(II), and Pd(II) complexes of an isoindoline pincer ligand: Consequences of steric crowding. *Inorg. Chem.* **2005**, *44*, 6476–6481.

(24) Esteruelas, M. A.; Gómez, A. V.; López, A. M.; Puerta, M. C.; Valera, P. Addition of ethyl diazoacetate to the allenylidene ligand of $[\text{Ru}(\eta^5\text{-C}_5\text{H}_5)(\text{C}=\text{C}=\text{CPh}_2)(\text{CO})(\text{PPR}'_2)]\text{BF}_4$: Synthesis of ruthenium organometallic compounds containing new cyclic unsaturated η^1 -carbon ligands. *Organometallics* **1998**, *17*, 4959–4965.

(25) Esteruelas, M. A.; Lahoz, F. J.; Oliván, M.; Oñate, E.; Oro, L. A. Azavinylidene and Azavinylidene-Bridged Compounds of Iridium and Rhodium. *Organometallics* **1994**, *13*, 3315–3323.

(26) (a) Andreu, P. L.; Cabeza, J. A.; del Río, I.; Riera, V.; Bois, C. Synthesis and reactivity of triruthenium carbonyl cluster complexes containing a bridging 1-azavinylidene ligand derived from benzophenone imine. *Organometallics* **1996**, *15*, 3004–3010. (b) Cabeza, J. A.; del Río, I.; Riera, V. Neutral and cationic diphenylphosphine and diphenylphosphido derivatives of a trinuclear ruthenium carbonyl cluster containing a bridging 1-azavinylidene ligand. *J. Organomet. Chem.* **1997**, *548*, 255–261. (c) Cabeza, J. A.; del Río, I.; Franco, R. J.; Grepioni, F.; Riera, V. Reactivity of a 1-azavinylidene ligand with diphenylacetylene on a ruthenium carbonyl cluster. A remarkable alkyne insertion into a metal-nitrogen bond. *Organometallics* **1997**, *16*, 2763–2764. (d) Cabeza, J. A.; del Río, I.; Moreno, M.; Riera, V.; Grepioni, F. Reactivity of a 1-azavinylidene-bridged triruthenium carbonyl cluster with alkynes. Synthesis of binuclear derivatives containing new C–H or C–N and C–C bonds formed by alkyne insertion into M–H or M–N and M–C bonds. *Organometallics* **1998**, *17*, 3027–3033. (e) Brown, S. N. Oxidative azavinylidene formation in the reaction of 1,3-diphenylisobenzofuran with osmium nitride complexes. *Inorg. Chem.* **2000**, *39*, 378–381. (f) Ruiz, J.; Rodríguez, V.; Cutillas, N.; Florenciano, F.; Pérez, J.; López, G. First complex containing a $\text{Pd}_2\mu_2(\text{-N}=\text{CPh}_2)_2$ functional group. *Inorg. Chem. Commun.* **2001**, *4*, 23–25. (g) Cabeza, J. A.; del Río, I.; Grepioni, F.; Moreno, M.; Riera, V.; Suárez, M. Reactivity of $[\text{Ru}_2\mu\text{-}\eta^1\text{-}\eta^1\text{-N}=\text{CPh}_2)(\mu\text{-}\eta^1\text{-}\eta^2\text{-PhC}=\text{CHPh})(\text{CO})_6]$ with alkynes. Insertion reactions of nonactivated alkynes into Ru–C and Ru–N bonds. *Organometallics* **2001**, *20*, 4190–4197. (h) Werner, H.; Müller, M.; Steinert, P. Synthesis, molecular structure and reactivity of neutral and cationic dinuclear iridium complexes with bridging azavinylidene ligands. *Z. Anorg. Allg. Chem.* **2003**, *629*, 1337–1346. (i) Ruiz, J.; Rodríguez, V.; Cutillas, N.; Hoffmann, A.; Chamayou, A. C.; Kazmierczak, K.; Janiak, C. Structure-solid-state CPMAS ^{13}C NMR correlation in palladacycle

solvates (pseudo-polymorphs) with a transformation from $Z' = 1$ to $Z' = 2$. *CrystEngComm* **2008**, *10*, 1928–1938.

(27) (a) Cowie, M.; Dwight, S. K. Binuclear Rhodium Complexes - Their Chemistry with Sulfur-Dioxide and the Structure of $[\text{Rh}_2\text{Cl}_2\mu(\text{SO}_2)((\text{C}_6\text{H}_5)_2\text{PCH}_2\text{P}(\text{C}_6\text{H}_5)_2)_2]$. *Inorg. Chem.* **1980**, *19*, 209–216. (b) Kang, S.-K.; Albright, T. A.; Wright, T. C.; Jones, R. A. The Bonding and Interconversion in a Series of $\text{Rh}_2(\text{CO})_4(\text{PR}_2)_2$ Isomers. *Organometallics* **1985**, *4*, 666–675. (c) Targos, T. S.; Geoffroy, G. L.; Rheingold, A. L. Binuclear Oxidative Addition of Alkynes to Phosphido-Bridged Dirhodium and Diiridium 1,5-Cyclooctadiene Complexes. *Organometallics* **1986**, *5*, 12–16. (d) Khoo, S.; Yeong, H.-X.; Li, Y. X.; Ganguly, R.; So, C.-W. Amidinate-Stabilized Group 9 Metal-Silicon(I) Dimer and -Silylene Complexes. *Inorg. Chem.* **2015**, *54*, 9968–9975.

(28) (a) Speck, K.; Magauer, T. The Chemistry of Isoindole Natural Products. *Beilstein J. Org. Chem.* **2013**, *9*, 2048–2078. (b) Albano, G.; Aronica, L. A. Potentiality and Synthesis of O- and N-Heterocycles: Pd-Catalyzed Cyclocarbonylative Sonogashira Coupling as a Valuable Route to Phthalans, Isochromans, and Isoindolines. *Eur. J. Org. Chem.* **2017**, 2017, 7204–7221.

(29) (a) Fernández, M. J.; Esteruelas, M. A.; Oro, L. A.; Apreda, M. C.; Foces-Foces, C.; Cano, F. H. Preparation, Properties, and Reactivity of Dihydridosilyl(nnnnnnnn^4 -Cycloocta-1,5-Diene)-Iridium(III) Complexes - X-Ray Crystal-Structures of the Dihydrido Silyl Complex $\text{IrH}_2(\text{SiEt}_3)(\mu^4\text{-C}_8\text{H}_{12})(\text{AsPh}_3)$ and the Cyclooctenyl Derivative $\text{Ir}(1\text{-}\sigma,4,5\text{-}\eta^2\text{-C}_8\text{H}_{13})(\text{CO})_2(\text{AsPh}_3)$. *Organometallics* **1987**, *6*, 1751–1756. (b) Bianchini, C.; Farnetti, E.; Graziani, M.; Nardin, G.; Vacca, A.; Zanobini, F. Electron-Rich Iridium Complexes with Mixed-Donor Polydentate Ligands - Chemoselective Catalysts in Hydrogen-Transfer Reduction of α,β -Unsaturated Ketones. *J. Am. Chem. Soc.* **1990**, *112*, 9190–9197. (c) Nguyen, D. H.; Greger, I.; Pérez-Torrente, J. J.; Jiménez, M. V.; Modrego, F. J.; Lahoz, F. J.; Oro, L. A. ONO Dianionic Pincer-Type Ligand Precursors for the Synthesis of α,β -Cyclooctenyl Iridium(III) Complexes: Formation Mechanism and Coordination Chemistry. *Organometallics* **2013**, *32*, 6903–6917. (d) Nguyen, D. H.; Pérez-Torrente, J. J.; Jiménez, M. V.; Modrego, F. J.; Gómez-Bautista, D.; Lahoz, F. J.; Oro, L. A. Unsaturated Iridium(III) Complexes Supported by a Quinolato-Carboxylato ONO Pincer-Type Ligand: Synthesis, Reactivity, and Catalytic C-H Functionalization. *Organometallics* **2013**, *32*, 6918–6930. (e) Padilla-Martínez, I. I.; Cervantes-Vásquez, M.; Leyva-Ramírez, M. A.; Paz-Sandoval, M. A. Iridaoxacyclohexadiene-Bridged Mixed-Valence Iridium Cyclooctadiene Complex: Oxidative Addition and Hydrogen-Transfer to Coordinated Cyclooctadiene. *Organometallics* **2014**, *33*, 6305–6318. (f) Boudreault, P.-L. T.; Esteruelas, M. A.; Mora, E.; Oñate, E.; Tsai, J.-Y. Pyridyl-Directed C–H and C–Br Bond Activations Promoted by Dimer Iridium-Olefin Complexes. *Organometallics* **2018**, *37*, 3770–3779.

(30) (a) Krinsky, J. L.; Arnold, J.; Bergman, R. G. Platinum group thiophenoxyimine complexes: Syntheses and crystallographic/computational studies. *Organometallics* **2007**, *26*, 897–909. (b) Kumaran, E.; How, K. T. S.; Ganguly, R.; Li, Y. X.; Leong, W. K. Synthesis and Reactivity of Cationic Iridium Aminocarbenes Derived from Terminal Alkynes and 2-Aminopyridines. *Organometallics* **2013**, *32*, 4149–4152. (c) Zumeta, I.; Mendicutie-Fierro, C.; Rodríguez-Diéguez, A.; Seco, J. M.; Garralda, M. A. Acyliridium(III) Complexes with PCN Terdentate Ligands Including Imino- or Iminium-Acyl Moieties or Formation of Hydrido from Hydroxyl. *Eur. J. Inorg. Chem.* **2016**, 2016, 1790–1797.

(31) (a) Esteruelas, M. A.; Oro, L. A. Dihydrogen complexes as homogeneous reduction catalysts. *Chem. Rev.* **1998**, *98*, 577–588. (b) Esteruelas, M. A.; López, A. M.; Mora, M.; Oñate, E. B–H formation and H–H formation: two consecutive heterolytic processes on an osmium-hydrogensulfide bond. *Chem. Commun.* **2013**, 49, 7543–7545. (c) Esteruelas, M. A.; López, A. M.; Oliván, M. Polyhydrides of Platinum Group Metals: Nonclassical Interactions and σ -Bond Activation Reactions. *Chem. Rev.* **2016**, *116*, 8770–8847.

(32) Giordano, G.; Crabtree, R. H. Di- μ -Chloro-Bis(η^4 -1,5-Cyclooctadiene)-Dirhodium(I). *Inorg. Synth.* **1974**, *19*, 88–90.

(33) Herde, J. L.; Lambert, J. C.; Senoff, C. V. Cyclooctene and 1,5-Cyclooctadiene Complexes of Iridium(I). *Inorg. Synth.* **1979**, *15*, 18–20.

(34) Usón, R.; Oro, L. A.; Cabeza, J. A. Dinuclear Methoxy, Cyclooctadiene, and Barrelene Complexes of Rhodium(I) and Iridium(I). *Inorg. Synth.* **1985**, *23*, 126–130.

(35) Green, L. M.; Meek, D. W. Synthesis, Characterization, and Reactivity of Alkoxide and Hydroxide Complexes of Rhodium(I) and Iridium(I). *Organometallics* **1989**, *8*, 659–666.

(36) Siegl, W. O. Metal-Ion Activation of Nitriles. Syntheses of 1,3-Bis(Arylimino)Isoindolines. *J. Org. Chem.* **1977**, *42*, 1872–1878.